Reaction of primary silanes with dinuclear rhodium hydride complexes: silane coupling reactions

Michael D. Fryzuk*, Lisa Rosenberg and Steven J. Rettig
Department of Chemistry, University of British Columbia, 2036 Main Mall, Vancouver, BC, V6T 1Z1 (Canada)

(Received January 27, 1994)

Abstract

The reaction of the dinuclear rhodium hydride dimer $[(dippe)Rh]_2(\mu\text{-}H)_2$ (dippe = 1,2-bis(diisopropylphosphino)ethane) with primary silanes is described. In the presence of two equivalents of $RSiH_3$ (R = Bu^n and Tol^p), dinuclear bis(μ-silylene) complexes of the formula $[(dippe)Rh]_2(\mu\text{-}SiHR)_2$ result. Attempts to generate silylhydride complexes of the formula $[(dippe)Rh]_2(\mu\text{-}H)(\mu\text{-}H\text{–}SiHR)$ by the addition of one equiv. of $RSiH_3$ failed. The bis(μ-silylene) complexes react with hydrogen to form adducts wherein two equivalents of H_2 per dimer unit have been activated; on the basis of NMR spectral studies these complexes are proposed to have the following formula: $[(dippe)RhH]_2(\mu\text{-}H\text{–}SiHR)_2$. These molecules are extremely fluxional and lose H_2 rather readily. Addition of more than three equivalents of primary silane to **1** generated dinuclear rhodium derivatives with three silicon-containing ligands, having the formula $[(dippe)Rh]_2(\mu\text{-}SiHR)(\mu\text{-}H\text{–}SiHR)_2$. In the presence of excess primary silane, the dinuclear rhodium hydride **1** acts as a catalyst precursor for the dehydrogenative coupling of silanes. With the *p*-tolylsilane, dimerization does occur but the process is complicated by disproportionation reactions to generate $(Tol^p)_2SiH_2$ and $(Tol^p)_3SiH$; with butylsilane, Si–Si chains with up to five silicons have been produced with no evidence of disproportionation. Crystals of $[(dippe)Rh]_2(\mu\text{-}SiHBu^n)_2$ (**2a**) are monoclinic, $a = 10.889(1)$, $b = 13.105(2)$, $c = 16.676(2)$ Å, $\beta = 104.06(1)°$, $Z = 2$, space group $P2_1/n$.; and those of $[(dippe)Rh]_2(\mu\text{-}\eta^2\text{-}H\text{–}SiHTol^p)_2(\mu\text{-}SiHTol^p)$ (**4b**) are monoclinic, $a = 25.839(4)$, $b = 13.084(3)$, $c = 17.133(3)$ Å, $\beta = 107.10(1)°$, $Z = 4$, space group $P2_1/a$. The structures were solved by Patterson (**2a**) and direct (**4b**) methods and were refined by full-matrix least-squares procedures to $R = 0.035$ and 0.047 ($R_w = 0.030$ and 0.060) for 3184 and 5997 reflections with $I \geq 3\sigma(I)$, respectively.

Key words: Crystal structures; Silane coupling reactions; Rhodium complexes; Hydride complexes; Dinuclear complexes

Introduction

The recent surge of interest in transition-metal silicon chemistry has been largely due to a desire to find new homogeneous catalysts for the preparation of Si–Si bonded polymers [1–3]. In the case of certain early transition-metal catalyst precursors based on zirconocene and titanocene derivatives, it has been shown that the reactivity and product chain length increase for different silanes in the order tertiary silanes (R_3SiH) < secondary silanes (R_2SiH_2) < primary silanes ($RSiH_3$) [3]. For this reason, attention has turned to the interaction of primary silanes with these metals, and derivatives have now been isolated which contain SiH_2R ligands, including the two examples shown below [4, 5]. The titanocene complex was isolated from a catalytic reaction mixture producing poly(phenylsilylene).

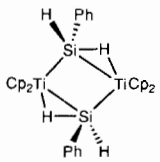

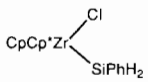

The use of late transition-metal catalysts for Si–Si bond-forming reactions has principally been limited to reactions with secondary silanes [6–8]. Dimers and trimers are the largest oligomers formed in these reactions. Tertiary silanes tend to be very unreactive towards dimerization, though traces of hexaethyldisilane were observed in reactions of a range of hydrosilation catalysts with triethylsilane [7]. The dehydrogenative coupling of $PhMe_2SiH$ to $(PhMe_2Si)_2$ catalyzed by platinum complexes has also been reported [9]. These

*Author to whom correspondence should be addressed.

Elsevier Science S.A.
SSDI 0020-1693(94)03927-G

small oligomeric silane coupling products are frequently accompanied by products of disproportionation reactions, a side reaction characteristic of late transition-metal catalyst precursors, particularly with arylsilanes.

A suggested mechanism for the dehydrogenative coupling of silanes by late transition-metal catalysts is based on oxidative–addition/reductive–elimination steps rather than by the σ bond metathesis processes that have been shown to be in effect for silane coupling by early transition metals [1, 10]. The former mechanism requires that at least two silyl groups be bound to the metal centre at some point for the coupling to occur; thus the steric requirements of the silane should affect the progress of the reaction.

The above results demonstrate that for both early and late transition-metal catalysts in dehydrogenative silicon–silicon coupling, sterics play an important role, yet not many examples exist of late transition-metal catalysts being used to oligomerize primary silanes. A study using Wilkinson's catalyst, $RhCl(PPh_3)_3$, did examine the behaviour of phenylsilane towards coupling, but found it behaved much as the secondary silanes did, giving dimers and trimers. Also observed were some products arising from coupling between phenylsilane and the disproportionation product, diphenylsilane [6]. Recently, though, there has been more interest in the reactions of late transition-metal complexes with primary silanes. Shown below are some complexes which are formed from the reaction of primary silanes with late transition-metal centres. Both of the platinum compounds were formed from mononuclear precursors, and both are catalyst precursors for at least slow dimerization of phenylsilane [11, 12]. The rhodium complex arises from the addition of a primary silane to a dinuclear hydride precursor. This complex is the subject of the only previous, in-depth study of the interactions of primary silanes with rhodium complexes. It is not, however, a catalyst precursor for dehydrogenative silicon coupling [13].

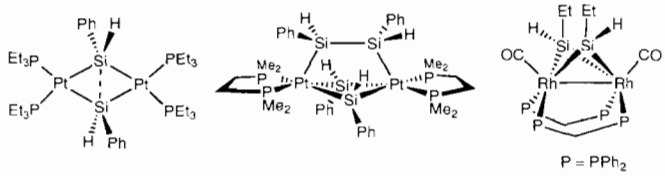

This paper describes the reactivity of the primary silanes, *p*-tolylsilane (Tol^pSiH_3) and n-butylsilane (Bu^nSiH_3), with the dinuclear rhodium hydride complex $[(dippe)Rh]_2(\mu\text{-}H)_2$ (**1**) (dippe = 1,2-bis(diisopropylphosphino)ethane).

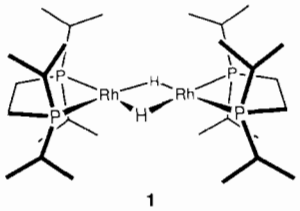

1

Previously, we reported [14] the reaction of this hydride dimer **1** with the secondary silane Ph_2SiH_2; in this case, **1** acts as a catalyst precursor for the coupling of Ph_2SiH_2 to $Ph_2HSi\text{–}SiHPh_2$. In this paper, the use of **1** as a catalyst precursor for the dehydrogenative coupling of these primary silanes is also described. Possible mechanisms for these catalytic cycles are discussed based on the stoichiometric chemistry observed and on product analysis of catalytic runs.

Experimental

General

All manipulations were performed under prepurified nitrogen in a Vacuum Atmospheres HE-553-2 workstation equipped with an MO-40-2H purification system or using Schlenk-type glassware. The term 'reactor bomb' refers to a cylindrical, thick-walled Pyrex vessel equipped with a 5 mm (or 10 mm, for larger bombs) Kontes Teflon needle valve and a ground glass joint for attachment to a vacuum line. NMR tubes used for preparing sealed samples are 8″ or 9″ Wilmad 507 PP NMR tubes with a female b14 joint attached by glassblowing.

Toluene and hexanes were pre-dried over CaH_2 then deoxygenated by distillation from molten sodium and sodium-benzophenone ketyl, respectively, under argon. Hexane used in the catalytic runs was spectroscopic grade, dried over sodium benzophenone ketyl and distilled under nitrogen. Pentane and diethyl ether were dried and deoxygenated by distillation from sodium benzophenone ketyl under argon. Di-n-butyl ether was dried by refluxing over CaH_2. Deuterated benzene (C_6D_6, 99.6 at.% D) and deuterated toluene (C_7D_8, 99.6 at.% D) were purchased from MSD Isotopes and dried over 4 Å molecular sieves. The dried, deuterated solvents were then degassed using three 'freeze–pump–thaw' cycles and were vacuum transferred before use. Deuterium gas was purchased from Matheson and passed through a glass coil immersed in liquid nitrogen to remove any traces of water and oxygen. Hydrogen gas was purified by being passed through a column packed with activated 4 Å molecular sieves and MnO.

^1H NMR spectra were recorded on Varian XL-300, Bruker WP-200, Bruker WH-400 or Bruker AMX-500

spectrometers. With d_6-benzene as solvent the spectra were referenced to C_6D_5H at 7.15 ppm and with d_8-toluene as solvent the spectra were referenced to the CD_2H residual proton at 2.09 ppm. $^{31}P\{^1H\}$ NMR spectra were recorded at 121.4 MHz on the Varian XL-300 or at 202.3 MHz on the Bruker AMX-500 and were referenced to external $P(OMe)_3$ at +141.0 ppm relative to 85% H_3PO_4. $^1H\{^{31}P\}$ NMR spectra were recorded on the Bruker AMX-500. $^2H\{^1H\}$ NMR spectra were run in C_6H_6 at 46.0 MHz on the Varian XL-300 and were referenced to residual solvent deuterons at 7.15 ppm. $^{29}Si\{^1H\}$ and ^{29}Si NMR were run at 59.6 MHz on the Varian XL-300 and were referenced to external TMS at 0.0 ppm.

Elemental analyses were carried out by Mr P. Borda of this department. Gas chromatography/mass spectrometry was carried out by Ms L. Madilao of this department.

The starting complex $[(dippe)Rh]_2(\mu\text{-}H)_2$ (**1**) was prepared using literature methods [15, 16]. The primary silanes n-butylsilane [17] and *p*-tolylsilane [18] were prepared by the $LiAlH_4$ reduction of the corresponding trichloroalkylsilanes. n-Butyltrichlorosilane and *p*-tolyltrichlorosilane were purchased from Petrarch Systems and used without further purification.

$[(dippe)Rh]_2(\mu\text{-}SiHBu^n)_2$ (2a)

To a stirred, dark green solution of $[(dippe)Rh]_2(\mu\text{-}H)_2$ (**1**) (94 mg, 0.128 mmol) in hexanes (4 ml) was added dropwise a solution of n-butylsilane (23 mg, 0.257 mmol) in hexanes (4 ml) to give a brownish red solution, which lightened in colour over 10 s, giving a golden yellow solution. The volume of the solution was reduced by one third. Slow evaporation of the solvent at room temperature overnight caused the solution to become red. Red crystals were obtained by cooling to −40 °C. Yield 67% (78 mg). NMR characterization showed these crystals to be a mixture of *trans* (85%) and *cis* (15%) isomers. The two isomers were inseparable by crystallization techniques, and heating or cooling solutions containing this mixture did not change the ratio of *trans* to *cis*. ^1H NMR (C_7D_8, ppm): Si–*H* (*trans*) 8.07 (br s); Si–*H* (*cis*) 7.58 (br s); total Si–*H* = 2H; $CH(CH_3)_2$, PCH_2CH_2P, $CH(CH_3)_2$, $CH_2CH_2CH_2CH_3$ 3.0–0.0 (overlapping br s and mult, 64H); distinguishable in this region was one set of signals due to $CH(CH_3)_2$: 1.22 (dd, ^3J(P–H) = 13.1, ^3J(H–H) = 7.1 Hz). $^{31}P\{^1H\}$ NMR (C_7D_8, ppm, $T = -35.5$ °C): *trans* 89.3 (d mult, ^1J(Rh–P) = 160 Hz); *cis* 86.7 (d mult, ^1J(Rh–P) = 158 Hz). *Anal.* Calc. for $C_{36}H_{84}P_4Rh_2Si_2$: C, 47.89; H, 9.38. Found: C, 48.23; H, 9.49%.

$[(dippe)Rh]_2(\mu\text{-}SiHTol^p)_2$ (2b)

To a stirred, dark green solution of $[(dippe)Rh]_2(\mu\text{-}H)_2$ (**1**) (131 mg, 0.179 mmol) in toluene (6 ml) was added dropwise a solution of *p*-tolylsilane (42 mg, 0.340 mmol, 1.9 equiv.) in toluene (6 ml) to give a brownish red solution, which lightened in colour over 10 s, giving a light orange solution. The volume of the solution was reduced by one third, during which time the solution colour darkened to a medium orange. A red–orange powder was obtained by cooling to −40 °C. Yield 65% (108 mg). Use of two, or slightly more than two, equivalents of the silane in this reaction tended to give small amounts of an impurity, $[(dippe)Rh]_2(\mu\text{-}\eta^2\text{-}H\text{–}SiHTol^p)_2(\mu\text{-}SiHTol^p)$, (**4b**). NMR characterization showed **2b** to be a mixture of *trans* (90%) and *cis* (10%) isomers. The two isomers were inseparable by crystallization techniques, and heating or cooling solutions containing this mixture did not change the ratio of *trans* to *cis*.

trans-2b. ^1H NMR (C_6D_6, ppm): Si–*H* 8.47 (mult, 2H); H_{ortho} 7.60 (br d, 4H); H_{meta} 6.99 (d, 4H, $3J$(H–H) = 7.8 Hz); $CH(CH_3)_2$ 2.80 (sept, 4H, ^3J(H–H) = 6.9 Hz); $SiC_6H_5CH_3$ 2.07 (s, 6H); $CH(CH_3)_2$ 1.95 (mult, 4H); $CH(CH_3)_2$ 1.45 (dd, 12H, ^3J(H–P) = 13.6, ^3J(H–H) = 6.8 Hz); PCH_2CH_2P 1.14 (mult, 8H); $CH(CH_3)_2$ 1.02 (dd, 12H, ^3J(H–P) = 9.2, ^3J(H–H) = 6.9 Hz); $CH(CH_3)_2$ 0.86 (dd, 12H, ^3J(H–P) = 13.8, ^3J(H–H) = 6.1 Hz); $CH(CH_3)_2$, 0.60 (dd, 12H, ^3J(H–P) = 14.8, $3J$(H–H) = 6.9 Hz). $^{31}P\{^1H\}$ NMR (C_6D_6, ppm: 91.0 (d mult, ^1J(Rh–P) = 159 Hz).

cis-2b. ^1H NMR (C_7D_8, ppm): this compound was never isolated separately from the *trans* isomer, and because it is present as approximately 10% of the *cis*/*trans* mixture, many of its signals in the ^1H NMR are buried beneath signals due to the *trans* isomer. The following were the only assignments made: H_{ortho} 7.99 (d, 4H, $^3J(H_o\text{–}H_m)$ = 7.5 Hz); Si–*H* 7.83 (br s, 2H). $^{31}P\{^1H\}$ NMR (C_7D_8, ppm): 88.2 (d mult, ^1J(Rh–P) = 153 Hz). *Anal.* Calc. for $C_{42}H_{80}P_4Rh_2Si_2$ (*trans* isomer): C, 51.95; H, 8.30. Found: C, 51.61; H, 8.23%.

Reaction of $[(dippe)Rh]_2(\mu\text{-}H)_2$ (1) with one equivalent n-butylsilane

To a solution of $[(dippe)Rh]_2(\mu\text{-}H)_2$ (**1**) (42 mg, 0.057 mmol) in toluene (3 ml) was added Bu^nSiH_3 (7 mg of a 70% solution in toluene, 0.056 mmol) in toluene (2 ml), dropwise, with stirring. The solution changed from a dark green to an orange–brown colour. The toluene was removed under vacuum and the residues were dissolved in d_6-benzene to make an NMR sample. The principal products, as determined by $^{31}P\{^1H\}$ NMR spectroscopy, were $[(dippe)Rh]_2(\mu\text{-}SiHBu^n)_2$ (**2a**) and $[(dippe)Rh]_2(\mu\text{-}H)_2$ (**1**). Repeating the reaction at low temperature (−70 °C) and warming the mixture to room temperature slowly did not change the results.

*Reaction of [(dippe)Rh]$_2$(μ-H)$_2$ (**1**) with one equivalent p-tolylsilane*

This reaction was carried out in the same manner as for the preceding reaction (76 mg, 0.10 mmol [(dippe)Rh]$_2$(μ-H)$_2$ (**1**); 13 mg, 0.10 mmol Tol^{p}SiH$_3$), with similar results. Repeating the reaction at low temperature (−70 °C) did not change the results.

*[(dippe)Rh(H)]$_2$(μ-η^2-H–SiHBu^n)$_2$ (**3a**)*

[(dippe)Rh]$_2$(μ-SiHBu^n)$_2$ (**2a**) (22 mg, 0.024 mmol) was dissolved in d$_8$-toluene in a sealable NMR tube. The tube was attached to a vacuum line by a needle valve adapter and slightly less than one atmosphere of hydrogen was introduced, after the solution was degassed by one freeze–pump–thaw cycle. The tube was tapped for 5–10 min to encourage diffusion of the gas into the red solution, which instantly lightened in colour to pale yellow. The tube was sealed and NMR spectra (^{1}H and ^{31}P{^{1}H}, variable temperature) of the sample were run. The ^{1}H NMR spectrum indicated the presence of two isomers in solution in approximately a 3:1 ratio. Because of fluxional processes which appear to be occurring, some of the rhodium hydride signal is not apparent in the room temperature spectrum. Also, no separate alkyl resonances for the minor (*trans*) isomer were observed; these resonances overlap with those for the major (*cis*) isomer. The ^{1}H NMR signals reported here are for the *cis* isomer, unless otherwise indicated. ^{1}H NMR (C$_7$D$_8$, ppm): Si–*H* 5.42 (br s); Si–*H* 5.03, 4.29 (br s, *trans* isomer) (total Si–*H* = 2H); C*H*(CH$_3$)$_2$ 1.96 (d sept, 8H, ^3J(H–H) = 6.8 Hz); SiCH$_2$C*H*$_2$CH$_2$CH$_3$ 1.83 (mult, 4H); SiCH$_2$CH$_2$C*H*$_2$CH$_3$ 1.58 (mult, 4H); PCH$_2$CH$_2$P 1.28 (d, 8H, ^2J(P–H) = 10.7 Hz); CH(C*H*$_3$)$_2$ 1.20 (dd, 24H, ^2J(P–H) = 14.7 Hz); CH(C*H*$_3$)$_2$ 1.05 (dd, 24H, ^2J(P–H) = 11.1 Hz); (these latter two signals cover those for n-butyl resonances totalling (10H); Rh–*H*, −11.85 (br s, 4H, $w_{1/2}$ = 90 Hz). ^{31}P{^{1}H} NMR (C$_7$D$_8$, ppm): 84.1 (br d, ^1J(Rh–P) = 117 Hz). Variable temperature NMR data are presented in 'Discussion'.

*[(dippe)Rh(H)]$_2$(μ-η^2-H–SiHTol^p)$_2$ (**3b**)*

This complex was prepared *in situ* in the same manner as described above for **3a**. The solution colour of the product is a slightly darker yellow colour than for **3a**. The product is approximately 75% *cis* and 25% *trans* isomer, as determined by ^{1}H NMR spectroscopy. Signals due to both isomers in the ^{1}H NMR spectrum are reported together. Due to the fluxionality of the isomers, accurate integrals of the Si–H signals could not be measured. ^{1}H NMR (C$_7$D$_8$, ppm): H$_{ortho}$ 8.00 (d, 4H, ^3J(H–H) = 7.8 Hz); Si–*H* 8.33–7.62 (br s buried under H$_{ortho}$ signal); H$_{meta}$ 7.08 (d, 4H); Si–*H* 5.36 (br s, $w_{1/2}$ = 27 Hz); H$_2$ (free), Si–*H* 4.51 (overlapping s and br s); SiC$_6$H$_5$C*H*$_3$ 2.15 (s, 6H); C*H*(CH$_3$)$_2$ 2.39–2.10 (br mult, 4H); C*H*(CH$_3$)$_2$, PC*H*$_2$C*H*$_2$P, CH(C*H*$_3$)$_2$ 1.95–0.34 (overlapping br s and mult, 60H); Rh–*H*, −5.12 (br s, $w_{1/2}$ = 190 Hz); Rh–*H*, −11.23 (br s, $w_{1/2}$ = 45 Hz); Rh–*H*, −12.45 (br s, $w_{1/2}$ = 190 Hz); total Rh–*H* = 4H. ^{31}P{^{1}H} NMR (C$_7$D$_8$, ppm): major isomer (*cis*, by analogy with **3a**): 102.5 (br s, $w_{1/2}$ = 450 Hz, 2P); 81.0 (br s, $w_{1/2}$ = 450 Hz); minor isomer (*trans*, by analogy with **3a**): 85.3 (asymmetric d mult). Variable temperature ^{31}P{^{1}H} NMR data are presented in 'Discussion'.

*Reaction of [(dippe)Rh(H)]$_2$(μ-η^2-H–SiHBu^n)$_2$ (**3a**) with deuterium*

A solution of [(dippe)Rh]$_2$(μ-SiHBu^n)$_2$ (**2a**) (35 mg, 0.039 mmol) in toluene (6 ml) was placed in a small reactor bomb and degassed by one freeze–pump–thaw cycle. Deuterium gas was introduced to one atmosphere. Over 10–15 s the solution colour changed from red–orange to a pale yellow. The solution was stirred under deuterium for 5 min, then the deuterium and toluene were removed under vacuum. The yellow residues were dissolved in d$_6$-benzene to make an NMR sample. Addition of the solvent caused the colour of the residues to darken slightly; ^{31}P{^{1}H} NMR spectroscopy confirmed the presence of a small amount of **2a**, though the bis(silylhydride) complex **3a** was the major product in solution. ^{1}H NMR spectroscopy showed the presence of small amounts of both silicon and rhodium hydrides in the sample, indicating the scrambling of the rhodium deuterides and the silicon hydrides from the original sample of **2a**.

*[(dippe)Rh]$_2$(μ-η^2-H–SiHBu^n)$_2$(μ-SiHBu^n) (**4a**)*

To a solution of [(dippe)Rh]$_2$(μ-H)$_2$ (**1**) (137 mg, 0.187 mmol) in pentane (5 ml) were added 5 equiv. of n-butylsilane (83 mg, 0.935 mmol) in pentane (4 ml). The colour of the solution immediately changed from dark green through brown to an intense yellow. A yellow powder was obtained from a minimum volume of pentane by cooling to −40 °C. Yield 62% (115 mg). ^{1}H NMR (C$_6$D$_6$, ppm, 500 MHz): Rh–H–Si*H*Bu^n 6.78 (br s, 1H, $w_{1/2}$ = 47 Hz, ^1J(Si–H) = 173 Hz*); Rh–H–Si*H*Bu^n 6.52 (br s, 1H, $w_{1/2}$ = 38 Hz, ^1J(Si–H) = 173 Hz*); μ-Si*H*Bu^n 4.59 (br s, 1H, $w_{1/2}$ = 35 Hz, ^1J(Si–H) = 165 Hz*); SiCH$_2$C*H*$_2$CH$_2$CH$_3$ 2.58–2.37 (overlapping mult, 6H); SiCH$_2$CH$_2$C*H*$_2$CH$_3$, C*H*(CH$_3$)$_2$ 2.25–1.84 (overlapping mult, 14H); SiC*H*$_2$CH$_2$CH$_2$C*H*$_3$, PC*H*$_2$C*H*$_2$P, CH(C*H*$_3$)$_2$ 1.80–0.99 (overlapping mult, 71H); Rh–*H* −8.03 (mult (second order), 1H, ^1J(Rh–H) = 24 Hz*); Rh–*H* −8.48 (mult (second order), 1H, ^1J(Rh–H) = 22 Hz). Parameters used in the simulation of the hydride region of **4a***: H$_a$ −8.04 (linewidth

*The simulation of the ^{31}P{^{1}H} NMR spectrum of **4a** was performed on a Macintosh IIx using NMR″ (Version 1.0) from Caleco Scientific Software Publishers.

5 Hz), H_b −8.48 (linewidth 4 Hz); $J(Rh_X–H_a)$ = 24 Hz, $J(P_A–H_a)$ = 11 Hz, $J(P_A–Rh_X)$ = 100 Hz, $J(P_M–H_a)$ = 13 Hz, $J(P_M–Rh_X)$ = 160 Hz, $J(Rh_Y–H_b)$ = 22 Hz, $J(P_B–H_b)$ = 13 Hz, $J(P_B–Rh_Y)$ = 100 Hz, $J(P_N–H_b)$ = 12 Hz, $J(P_N–Rh_Y)$ = 160 Hz. $^{31}P\{^1H\}$ NMR (C_6D_6, ppm, 121.4 MHz, room temperature): 87.4

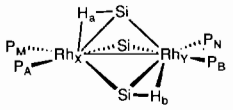

(br d mult, 1P, $^1J(Rh–P)$ = 160 Hz); 82.7 (br d mult, 1P, $^1J(Rh–P)$ = 155 Hz); 62.8 (br d, 1P, $^1J(Rh–P)$ = 102 Hz); 60.6 (br d, 1P, $^1J(Rh–P)$ = 104 Hz). Variable temperature $^{31}P\{^1H\}$ NMR spectra are presented in 'Discussion'. Parameters used for simulation of the $^{31}P\{^1H\}$ NMR spectrum observed for **4a** in C_7D_8 at −24 °C: P_A 63.21 (linewidth 7 Hz), P_B 60.76 (linewidth 5 Hz), P_M 88.56 (linewidth 10 Hz), P_N 83.13 (linewidth 10 Hz); $J(X–A)$ = 106, $J(Y–B)$ = 105, $J(A–B)$ = 10, $J(X–M)$ = 163, $J(Y–N)$ = 161, $J(M–N)$ = 53 Hz. ^{29}Si NMR (C_6D_6, ppm): 125.5 (br t, 2Si, $^1J(H–Si\ av.)$ = 180 Hz); 90.2 (br mult, 1Si). *Anal.* Calc. for $C_{40}H_{96}P_4Rh_2Si_3$: C, 48.47; H, 9.76. Found: C, 48.77; H, 9.89%.

*[(dippe)Rh]$_2$(μ-η^2-H–SiHTol^p)$_2$(μ-SiHTol^p) (**4b**)*

To a solution of [(dippe)Rh]$_2$(μ-H)$_2$ (**1**) (86 mg, 0.117 mmol) in hexanes (4 ml) were added 4 equiv. of *p*-tolylsilane (57 mg, 0.466 mmol) in pentane (3 ml). The colour of the solution immediately changed from dark green through brown to a light golden orange. Light orange needles were obtained from a minimum volume of hexanes by cooling to −40 °C. Yield 84% (108 mg). ^1H NMR (C_7D_8, ppm): H(*ortho*) 8.15 (br d, 6H); H(*meta*) 7.07 (d, 6H, $^3J(H_o–H_m)$ = 7.5 Hz); Si–*H* 7.58–6.41 (br s, 3H); $SiC_6H_5CH_3$ 2.18 (s, 9H); $CH(CH_3)_2$, PCH_2CH_2P, $CH(CH_3)_2$ 2.07–0.61 (overlapping mult, 64H) [distinguishable in this region are: $CH(CH_3)_2$ 1.80 (mult); $CH(CH_3)_2$ 1.38 (dd, $^3J(P–H)$ = 14.7, $^3J(H–H)$ = 6.9 Hz); $CH(CH_3)_2$ 0.76 (dd, $^3J(P–H)$ = 11.8, $^3J(H–H)$ = 6.7 Hz)]; Rh–*H* −6.89 (mult (second order), 2H, $^1J(H–Rh)$ = 25 Hz). ^1H NMR (C_7D_8, ppm, T = −45 °C): H_{ortho} 8.74 (br d, 1H); Si–*H*, H_{ortho} 8.56–8.26 (overlapping br mult and br d, 4H, $^3J(H_o–H_m)$ = 6.3 Hz); H_{ortho} 8.12 (br d, 2H, $^3J(H_o–H_m)$ = 6.6 Hz); H_{ortho} 7.95 (br d, 1H, $^3J(H_o–H_m)$ = 6.9 Hz); H_{meta} 7.45–6.90 (overlapping br d, 6H); Si–*H* 5.74 (br s, 1H, $w_{1/2}$ = 33 Hz); $SiC_6H_5CH_3$ 2.26 (s, 3H); $SiC_6H_5CH_3$ 2.18 (s, 3H); $SiC_6H_5CH_3$ 2.215 (s, 3H); $CH(CH_3)_2$, PCH_2CH_2P, $CH(CH_3)_2$ 1.98–0.43 (overlapping mult, 64H); Rh–*H* −6.91 (br mult, 2H). $^{31}P\{^1H\}$ NMR (C_7D_8, ppm): 90–55 (br, 2P); 70.6 (br s, 2P, $w_{1/2}$ = 760 Hz). $^{31}P\{^1H\}$ NMR (C_7D_8, ppm, T = −30 °C): 85.0 (dd, 1P, $^1J(Rh–P)$ = 158, $^3J(P–P)$ = 24 Hz); 77.6 (dd, 1P, $^1J(Rh–P)$ = 1170 Hz); 64.8 (d, 1P, $^1J(Rh–P)$ = 121 Hz); 55.4 (d, 1P, $^1J(Rh–P)$ = 121 Hz). Other variable temperature $^{31}P\{^1H\}$ NMR spectra are presented in 'Discussion'. ^{29}Si NMR (C_6D_6, ppm): 142–100 (br). *Anal.* Calc. for $C_{49}H_{90}P_4Rh_2Si_3$: C, 53.84; H, 8.30. Found: C, 53.89; H, 8.24%.

Catalytic coupling of p-tolylsilane

A typical procedure for the coupling reaction is as follows. In a 75 ml reactor bomb was placed *p*-tolylsilane (168 mg, 1.38 mmol) in 2.50 ml toluene, along with a stir bar. Addition by syringe of a dark green solution of [(dippe)Rh]$_2$(μ-H)$_2$ (**1**) (0.25 ml of a 0.055 M solution in toluene, 0.014 mmol) to the substrate solution gave an immediate colour change to golden, accompanied by the evolution of bubbles (H_2). The mixture was allowed to stir for approximately two days open to the nitrogen manifold, which was vented to a nujol bubbler to allow H_2 produced in the reaction to escape. Two days after the catalyst was added to the substrate solution the bomb was taken into a glovebox, where the mixture was passed down a Florisil column to remove the catalyst.

The eluted reaction products were analyzed by GC-MS. The consumption of monomer was low, 36% based on products observed in the GC trace. The major product was 1,2-di-*p*-tolyldisilane; other products included di-*p*-tolylsilane, tri-*p*-tolylsilane and 1,1,2-tri-*p*-tolyldisilane. Parent ions observed for these products in the mass spectra are shown in the table below. Evidently SiH_4 is forming during the disproportionation reactions but is carried away by the hydrogen evolved during the reaction.

Catalytic coupling of n-butylsilane

A typical procedure for the coupling reaction is as follows. In a 75 ml reactor bomb was placed [(dippe)Rh]$_2$(μ-H)$_2$ (**1**) (14 mg, 0.019 mmol) in 2.0 ml hexane, along with a stir bar. Addition of Bu^nSiH_3 (165 mg, 1.87 mmol) in 2.0 ml hexane to the dark green catalyst solution gave an immediate colour change to yellow, accompanied by the evolution of bubbles (H_2). The head space in the bomb was evacuated several times, causing an increase in the bubbling which continued (with successive head space evacuation) for several hours. The mixture was allowed to stir overnight open to the nitrogen manifold, which was vented to a nujol bubbler to allow H_2 produced in the reaction to escape. 24 h after the substrate was added to the

Products	Tol^pSiH_3	$(Tol^p)_2SiH_2$	$(Tol^pSiH_2)_2$	$(Tol^p)_3SiH$	$Tol^pSiH_2–SiH(Tol^p)_2$
M^+ (*m/e*)	122	212	242	302	332

catalyst the bomb was taken into a glovebox, where the mixture was passed down a Florisil column to remove the catalyst.

The eluted reaction products were analyzed by GC-MS. The consumption of monomer was 63%, and the products were obtained in the following quantities: 18.9% disilane, 29.4% trisilane, 12.9% tetrasilane (two diastereomers in approximately a 5:1 ratio) and 1.8% pentasilane (two peaks in a 1:1 ratio, probably both linear products). The mass spectral data were in agreement with those reported from an earlier study of the polymerization of n-butylsilane [19]. The GC response factors for these polysilanes have not been measured, so the relative integrals from the GC trace, and therefore the yields, are uncorrected.

Calculation of $\Delta G^{\ddagger}$ for the phosphine and hydride exchange in 3a

$\Delta G^{\ddagger}$ was calculated using the value for the rate constant [20] k_c (where $k_c = \pi\Delta\nu_c/(2)^{1/2}$) in the Eyring equation, $\Delta G^{\ddagger} = -RT_c \ln[(k_c h)/(k_B T_c)]$, where R = the gas constant, T_c = temperature of coalescence, $\Delta\nu_c$ = peak separation at the low T limit, h = Planck's constant and k_B = Boltzmann constant.

For the phosphorus resonances due to the major isomer in the variable temperature $^{31}P\{^1H\}$ NMR spectra of **3a**. $T_c = 253$ K (−20 °C) and $\Delta\nu_c = 2.00 \times 10^3$ Hz. The coalescence temperature was estimated visually from the spectra and has an error of approximately ±5 K.

For the hydride resonances due to the major isomer in the variable temperature ^1H NMR spectra of **3a**, $T_c = 263$ K (−10 °C) and $\Delta\nu_c = 797$ Hz. The coalescence temperature was estimated visually from the spectra and has an error of approximately ±5 K.

X-ray crystallographic analyses of [(dippe)Rh]$_2$(μ-SiHBu^n)$_2$ (2a) and [(dippe)Rh]$_2$(μ-η^2-H–SiH$_2$Tol^p)$_2$(μ-SiHTol^p) (4b)

Crystallographic data appear in Table 1. The final unit-cell parameters were obtained by least-squares on the setting angles for 25 reflections with $2\theta = 23.2$–$28.0°$ and 24.0–36.1° for **2a** and **4b** respectively. The intensities of three standard reflections, measured every 200 reflections throughout the data collections, remained constant for **2a** and decayed uniformly and linearly by 32.5% for **4b**. The data were processed [21], corrected for Lorentz and polarization effects, decay (for **4b**), and absorption (empirical: based on azimuthal scans for three reflections).

The structure of **2a** was solved by conventional heavy atom methods and that of **4b** was solved by direct methods. The dinuclear complex **2a** has exact inversion symmetry. The non-hydrogen atoms of both structures were refined with anisotropic thermal parameters. The silyl hydride atom of **2a** was refined with an isotropic thermal parameter and the silyl hydride atoms of **4b** were placed in difference map positions but were not refined. All other hydrogen atoms were fixed in idealized positions (staggered methyl groups, C–H = 0.98 Å for **2a** and 0.99 Å for **4b**, $B_H = 1.2B_{\text{bonded atom}}$). Corrections for secondary extinction (Zacharaisen type) were applied, the final values of the extinction coefficients being $2.5(3) \times 10^{-7}$ for **2a** and $9.4(8) \times 10^{-8}$ for **4b**. Neutral atom scattering factors and anomalous dispersion corrections for all atoms were taken from the International Tables for X-Ray Crystallography [22]. Final atomic coordinates and equivalent isotropic thermal parameters are given in Tables 2 and 3, and selected bond lengths and angles appear in Tables 4 and 5, and Tables 6 and 7, respectively. See also 'Supplementary material'.

Results and discussion

Stoichiometric reactions of [(dippe)Rh]$_2$(μ-H)$_2$ (1) with primary silanes

Preparation of the bis(μ-silylene) complexes [(dippe)Rh]$_2$(μ-SiHR)$_2$ (R = Bu^n (2a), Tol^p (2b))

Addition of 2 equiv. of primary silane to [(dippe)Rh]$_2$(μ-H)$_2$ (**1**) initially causes a colour change from dark green to yellow. Over 10–15 min the solution colour gradually darkens to orange, and if the mixture is left at room temperature for several hours or more it eventually changes to red (for n-butylsilane) or red–orange (*p*-tolylsilane). Air and moisture sensitive red–orange crystals of the bis(μ-silylene) complexes [(dippe)Rh]$_2$(μ-SiHR)$_2$ (R = Bu^n (**2a**), Tol^p (**2b**)) are isolated from these solutions.

$$\underset{\mathbf{1}}{[(\text{dippe})\text{Rh}]_2(\mu\text{-H})_2} + 2\text{RSiH}_3 \xrightarrow[-3\text{H}_2]{} [(\text{dippe})\text{Rh}]_2(\mu\text{-SiHR})_2 \quad (1)$$

2a: R = Bu^n
2b: R = Tol^p

Silyl hydride complexes of the formula [(dippe)Rh]$_2$(μ-H)(μ-η^2-H–SiHR), where R = Bu^n or Tol^p, could not be isolated. This is contrast to our earlier work wherein addition of 1 equiv. of the secondary silane, Ph_2SiH_2, to **1** resulted in the formation of the silyl hydride complex [(dippe)Rh]$_2$(μ-H)(μ-η^2-H–SiPh$_2$) [14, 23]. Addition of a single equivalent of primary silane to a dark green toluene solution of [(dippe)Rh]$_2$(μ-H)$_2$ (**1**) generates a brownish green solution; ^1H and $^{31}P\{^1H\}$ NMR spectra indicate that the major species in this reaction mixtures are the starting hydride dimer and a mixture of isomers of the bis(μ-silylene) complex [(dippe)Rh]$_2$(μ-SiHR)$_2$ (**2**). The same results were achieved even when the reaction was carried out at −70 °C and the mixture was allowed

TABLE 1. Crystallographic data[a]

Compound	[(dippe)Rh]$_2$(μ-SiHBu^n)$_2$ (**2a**)	[(dippe)Rh]$_2$(μ-η^2-H–SiH$_2$Tol^p)$_2$(μ-SiHTol^p) (**4b**)
Formula	$C_{36}H_{84}P_4Rh_2Si_2$	$C_{49}H_{90}P_4Rh_2Si_3$
Formula weight	902.94	1093.21
Color, habit	red, plate	orange, prism
Crystal size, mm	0.06×0.25×0.30	0.10×0.18×0.35
Crystal system	monoclinic	monoclinic
Space group	$P2_1/n$	$P2_1/a$
a (Å)	10.889(1)	25.839(4)
b (Å)	13.195(2)	13.084(3)
c (Å)	16.676(2)	17.133(3)
β (°)	104.06(1)	107.10(1)
V (Å^3)	2308.3(6)	5535(1)
Z	2	4
T (°C)	21	21
D_c (g/cm^3)	1.299	1.312
F(000)	956	2304
Radiation	Mo	Cu
μ (cm^{-1})	9.13	67.56
Transmission factors	0.89–1.00	0.81–1.00
Scan type	ω–2θ	ω–2θ
Scan range (° in ω)	1.26+0.35 tan θ	0.90+0.20 tan θ
Scan speed (°/min)	16 (up to 8 rescans)	16 (up to 8 rescans)
Data collected	$+h$, $+k$, $\pm l$	$+h$, $+k$, $\pm l$
$2\theta_{max}$ (°)	60	120
Crystal decay (%)	negligible	32.5
Total no. reflections	7348	8873
Unique reflections	7017	8657
R_{merge}	0.045	0.037
No. with $I \geq 3\sigma(I)$	3184	5997
No. of variables	204	524
R	0.035	0.047
R_w	0.030	0.060
GOF	1.59	2.13
Max. Δ/σ (final cycle)	0.005	0.02
Residual density (e/Å^3)	−0.44, 0.49	−0.83, 1.11 (near Rh)

[a]Rigaku AFC6S diffractometer, takeoff angle 6.0°, aperture 6.0×6.0 mm at a distance of 285 mm from the crystal, stationary background counts at each end of the scan (scan/background time ratio 2:1), Mo Kα radiation (λ = 0.71069 Å) or Cu Kα radiation (λ = 1.54178 Å), graphite monochromator, $\sigma^2(F^2) = [S^2(C+4B)]/L_p^2$ (S = scan speed, C = scan count, B = normalized background count), function minimized $\Sigma w(|F_o| - |F_c|)^2$ where $w = 4F_o^2/\sigma^2(F_o^2)$, $R = \Sigma||F_o| - |F_c||/\Sigma|F_o|$, $R_w = (\Sigma w(|F_o| - |F_c|)^2/\Sigma w|F_o|^2)^{1/2}$, and $GOF = [\Sigma w(|F_o| - |F_c|)^2/(m-n)]^{1/2}$. Values given for R, R_w, and GOF are based on those reflections with $I \geq 3\sigma(I)$.

to warm to room temperature slowly. Since we have previously shown that the diphenylsilyl hydride complex [(dippe)Rh]$_2$(μ-H)(μ-η^2-H–SiPh$_2$) is an intermediate in the formation of the bis(diphenylsilylene) derivative [(dippe)Rh]$_2$(μ-SiPh$_2$)$_2$, presumably the corresponding primary silyl hydride complexes [(dippe)Rh]$_2$(μ-H)(μ-η^2-H–SiHR) are forming upon addition of silane to the hydride dimer **1**, but evidently they react more quickly with free silane than does the hydride dimer.

Solid-state structure of trans-[(dippe)Rh]$_2$(μ-SiHBu^n)$_2$ (2a)

An X-ray crystallographic analysis was carried out on a crystal of [(dippe)Rh]$_2$(μ-SiHBu^n)$_2$ (**2a**) which turned out to be the *trans* geometric isomer. An ORTEP diagram of the molecular structure of *trans*-**2a** is shown in Fig. 1, and some relevant bond lengths and bond angles are shown in Tables 4 and 5, respectively.

The dimensions of this bis(μ-silylene) structure are typical of dimeric M_2Si_2 complexes [24, 25]. The Si–Si separation of 3.671 Å in the planar core of *trans*-**2a** is however much longer than that of 2.575(15) Å found for [(Et$_3$P)$_2$Pt]$_2$(μ-SiHPh)$_2$ for which an Si–Si interaction is proposed.

Solution NMR spectra of [(dippe)Rh]$_2$(μ-SiHR)$_2$ (R = Bu^n (2a), Tol^p (2b))

The room temperature $^{31}P\{^1H\}$ NMR spectra of complexes **2a,b** show signals attributable to the presence of two isomers in solution. The signals have been tentatively assigned to *cis* and *trans* geometric isomers of **2a** and **2b**. If the assignments are correct and the *trans* isomer is the major form, then the ratio of *trans* to *cis* isomers is 85:15 for **2a** and 9:1 for **2b**. Heating these samples in d$_8$-toluene at 80 °C for a week showed no change in this ratio.

TABLE 2. Final atomic coordinates (fractional) and B_{eq} (Å^2) for [(dippe)Rh]$_2$(μ-SiHBu^n)$_2$ (**2a**)

Atom	*x*	*y*	*z*	B_{eq}[a]
Rh(1)	0.50583(3)	0.44073(2)	0.42813(2)	3.00(1)
P(1)	0.3833(1)	0.42203(9)	0.29814(6)	3.81(5)
P(2)	0.6393(1)	0.3234(1)	0.39536(7)	4.00(5)
Si(1)	0.5868(1)	0.3994(1)	0.56707(7)	3.67(5)
C(1)	0.4415(5)	0.3072(4)	0.2527(3)	5.6(2)
C(2)	0.5821(5)	0.2937(4)	0.2833(3)	5.6(2)
C(3)	0.2153(4)	0.3835(4)	0.2854(3)	5.1(2)
C(4)	0.3692(4)	0.5198(3)	0.2154(3)	4.7(2)
C(5)	0.6659(4)	0.1938(3)	0.4419(3)	4.8(2)
C(6)	0.8045(4)	0.3661(4)	0.3997(3)	5.6(3)
C(7)	0.2019(5)	0.3102(5)	0.3523(4)	8.0(3)
C(8)	0.1227(5)	0.4719(5)	0.2824(3)	7.2(3)
C(9)	0.4990(5)	0.5550(4)	0.2088(3)	6.3(3)
C(10)	0.2887(6)	0.4889(4)	0.1290(3)	7.6(3)
C(11)	0.5403(5)	0.1386(4)	0.4295(3)	6.3(3)
C(12)	0.7635(5)	0.1269(4)	0.4131(3)	7.4(3)
C(13)	0.8049(5)	0.4709(4)	0.3602(4)	8.5(4)
C(14)	0.8896(5)	0.3669(5)	0.4867(4)	8.9(4)
C(15)	0.5117(5)	0.2870(3)	0.6097(3)	4.6(2)
C(16)	0.3686(5)	0.2772(3)	0.5821(3)	5.0(2)
C(17)	0.3118(6)	0.1826(4)	0.6112(4)	7.0(3)
C(18)	0.1703(6)	0.1768(5)	0.5774(4)	7.8(3)

[a] $B_{eq} = (8/3)\pi^2\Sigma\Sigma U_{ij}a^*_i a^*_j(\mathbf{a}_i \cdot \mathbf{a}_j)$.

The room temperature ^{1}H NMR spectra of these complexes are consistent with the bis(μ-silylene) structure, with resonances due to the terminal silicon hydrides occurring between 8.5 and 7.5 ppm. For both **2a** and **2b** the Si–H resonances of the *cis* isomer are at higher field (by roughly 0.5 ppm) than the *trans* isomer. These ^{1}H NMR spectra are slightly complex because there is a mixture of approximately 85–90% *trans* isomer and 10–15% *cis* isomer in solution. It is not possible to pick out all peaks due to the *cis* isomers because of overlap with the signals due to the *trans* isomers. For **2a** the room temperature spectrum is broad and poorly resolved. This may be due to some fluxionality arising from the motion of the n-butyl chain. Cooling the sample does not substantially improve the resolution.

*Formation of the bis(silylhydride) complexes [(dippe)Rh(H)]$_2$(μ-η^2-H–SiHR)$_2$ (R = Bu^n (**3a**), Tol^p (**3b**))*

As was mentioned above, when 2 equiv. of a primary silane are added to [(dippe)Rh]$_2$(μ-H)$_2$ (**1**) the solutions initially turn yellow, then gradually darken to red (**2a**) or red–orange (**2b**). The initial, yellow product is thought to be a bis(silylhydride) adduct, directly analogous to the bis(dimethylsilylhydride) complex, [(dippe)Rh(H)]$_2$-(μ-η^2-H–SiMe$_2$)$_2$, which was previously isolated and crystallographically characterized [23]. This adduct, **3**,

TABLE 3. Atomic coordinates and B_{eq} for [(dippe)Rh]$_2$(μ-η^2-H–SiHTol^p)$_2$(μ-SiHTol^p) (**4b**)

Atom	*x*	*y*	*z*	B_{eq}[a]
Rh(1)	0.19907(2)	0.11436(4)	0.21085(3)	3.41(1)
Rh(2)	0.17244(2)	0.31972(4)	0.23905(3)	3.41(1)
P(1)	0.28240(8)	0.0388(2)	0.2031(1)	5.04(5)
P(2)	0.15925(8)	−0.0329(1)	0.1461(1)	4.54(5)
P(3)	0.22886(8)	0.4648(1)	0.2839(1)	4.39(4)
P(4)	0.10523(8)	0.4141(2)	0.2678(1)	4.47(5)
Si(1)	0.11339(7)	0.1789(2)	0.2031(1)	3.62(4)
Si(2)	0.19254(8)	0.2484(2)	0.1172(1)	3.63(4)
Si(3)	0.21970(8)	0.2054(1)	0.3410(1)	3.76(4)
C(1)	0.2617(4)	−0.0828(7)	0.1479(7)	7.7(3)
C(2)	0.2124(4)	−0.1286(7)	0.1619(6)	6.9(3)
C(3)	0.3314(4)	−0.0042(8)	0.3008(7)	7.5(3)
C(4)	0.3245(4)	0.0894(9)	0.1390(8)	8.8(4)
C(5)	0.1094(4)	−0.1002(7)	0.1852(7)	7.1(3)
C(6)	0.1302(5)	−0.0289(7)	0.0311(6)	7.6(3)
C(7)	0.3046(6)	−0.067(1)	0.3530(8)	11.8(5)
C(8)	0.3812(4)	−0.0609(10)	0.2939(9)	10.5(4)
C(9)	0.3419(10)	0.039(2)	0.087(1)	24(1)
C(10)	0.3602(5)	0.1772(9)	0.1784(7)	8.8(4)
C(11)	0.1316(6)	−0.1211(8)	0.2755(8)	10.0(4)
C(12)	0.0872(5)	−0.2001(8)	0.1405(10)	11.7(5)
C(13)	0.0725(5)	0.0094(8)	0.0052(7)	10.5(4)
C(14)	0.1383(6)	−0.117(1)	−0.0173(7)	11.2(4)
C(15)	0.1825(3)	0.5705(6)	0.2879(6)	5.7(2)
C(16)	0.1336(3)	0.5362(6)	0.3142(5)	5.7(2)
C(17)	0.2649(3)	0.5238(6)	0.2166(5)	5.7(2)
C(18)	0.2803(3)	0.4774(6)	0.3863(5)	5.2(2)
C(19)	0.0678(3)	0.3718(7)	0.3403(5)	5.4(2)
C(20)	0.0479(3)	0.4617(6)	0.1810(5)	5.6(2)
C(21)	0.2294(4)	0.5410(7)	0.1293(6)	7.4(3)
C(22)	0.3147(4)	0.4610(7)	0.2157(6)	6.5(3)
C(23)	0.2552(4)	0.4537(7)	0.4549(5)	6.5(2)
C(24)	0.3112(4)	0.5785(7)	0.4029(6)	7.2(3)
C(25)	0.1077(4)	0.3420(8)	0.4233(6)	7.3(3)
C(26)	0.0264(4)	0.4484(8)	0.3533(7)	8.5(3)
C(27)	0.0676(3)	0.5164(7)	0.1155(6)	6.2(2)
C(28)	0.0069(3)	0.3794(7)	0.1426(6)	6.8(3)
C(29)	0.0677(3)	0.1257(5)	0.2619(4)	3.9(2)
C(30)	0.0844(3)	0.0939(7)	0.3428(5)	5.2(2)
C(31)	0.0488(3)	0.0531(7)	0.3814(5)	5.5(2)
C(32)	−0.0055(3)	0.0441(6)	0.3404(5)	5.0(2)
C(33)	−0.0230(3)	0.0727(7)	0.2602(5)	5.2(2)
C(34)	0.0127(3)	0.1135(6)	0.2212(5)	4.8(2)
C(35)	−0.0444(3)	−0.0002(7)	0.3830(5)	6.1(2)
C(36)	0.1464(3)	0.2499(5)	0.0079(4)	4.2(2)
C(37)	0.1638(3)	0.2119(6)	−0.0548(5)	4.9(2)
C(38)	0.1300(4)	0.2085(6)	−0.1354(5)	5.6(2)
C(39)	0.0778(4)	0.2431(6)	−0.1566(5)	5.3(2)
C(40)	0.0610(3)	0.2841(6)	−0.0941(5)	5.4(2)
C(41)	0.0930(3)	0.2868(6)	−0.0148(5)	4.8(2)
C(42)	0.0407(4)	0.2369(7)	−0.2420(5)	7.1(3)
C(43)	0.2942(3)	0.2199(5)	0.3997(4)	3.8(2)
C(44)	0.3133(3)	0.2103(6)	0.4838(5)	5.2(2)
C(45)	0.3688(4)	0.2199(7)	0.5252(5)	6.4(2)
C(46)	0.4057(4)	0.2387(7)	0.4827(6)	6.1(2)
C(47)	0.3869(3)	0.2509(6)	0.4002(5)	5.2(2)
C(48)	0.3322(3)	0.2416(6)	0.3588(4)	4.6(2)
C(49)	0.4654(4)	0.2451(9)	0.5292(8)	9.8(4)

[a] $B_{eq} = \frac{8}{3}\pi^2(U_{11}(aa^*)^2 + U_{22}(bb^*)^2 + U_{33}(bb^*)^2 + 2U_{12}aa^*bb^* \cos\gamma + 2U_{13}aa^*cc^* \cos\beta + 2U_{23}bb^*cc^* \cos\alpha)$.

TABLE 4. Selected bond lengths for *trans*-[(dippe)Rh]$_2$(μ-SiHBu^n)$_2$ (**2a**)

Bond	Length (Å)	Bond	Length (Å)	Bond	Length (Å)
Rh1–Rh1^a	2.8850(7)	Rh1–Si1	2.334(1)	Si1–C15	1.905(5)
Rh1–P1	2.266(1)	Rh1–Si1^a	2.335(1)	C15–C16	1.519(6)
Rh1–P2	2.272(1)	Si1–H1	1.45(3)		

^{a}Refer to symmetry operation: $1-x$, $1-y$, $1-z$.

TABLE 5. Selected bond angles for *trans*-[(dippe)Rh]$_2$(μ-SiHBu^n)$_2$ (**2a**)

Bonds	Angle (°)	Bonds	Angle (°)
P1–Rh1–P2	87.64(4)	Rh1–Si1–C15	117.2(1)
Si1–Rh1–Si1^a	103.66(4)	Rh1^a–Si1–C15	116.9(1)
Rh1–Si1–Rh1^a	76.34(4)		

^{a}Refer to symmetry operation: $1-x$, $1-y$, $1-z$.

TABLE 6. Selected bond lengths for [(dippe)Rh]$_2$(μ-η^2-H–SiHTol^p)$_2$(μ-SiHTol^p) (**4b**)

Bond	Length (Å)	Bond	Length (Å)	Bond	Length (Å)
Rh1–Rh2	2.8499(9)	Rh2–P3	2.379(2)	Rh2–H2	1.47
Rh1–P1	2.409(2)	Rh2–P4	2.299(2)	Si1–H1	1.41
Rh1–P2	2.309(2)	Rh2–Si1	2.356(2)	Si2–H2	1.47
Rh1–Si1	2.336(2)	Rh2–Si2	2.477(2)	Si2–H3	1.31
Rh1–Si2	2.349(2)	Rh2–Si3	2.350(2)	Si3–H4	1.43
Rh1–Si3	2.444(2)	Rh1–H4	1.49	Si3–H5	1.39

TABLE 7. Selected bond angles for [(dippe)Rh]$_2$(μ-η^2-H–SiHTol^p)$_2$(μ-SiHTol^p) (**4b**)

Bonds	Angle (°)	Bonds	Angle (°)
P1–Rh1–P2	84.84(7)	Rh1–Si2–Rh2	72.34(5)
P3–Rh2–P4	86.10(7)	Rh1–Si3–Rh2	72.92(6)
P1–Rh1–Si1	173.13(7)	C29–Si1–H1	97.9
P3–Rh2–Si1	175.38(7)	C36–Si2–H3	100.6
Rh1–Si1–Rh2	74.79(6)	C43–Si3–H5	72.3

would result from addition of a second equivalent of silane to the unobserved, highly reactive silyl hydride complex [(dippe)Rh]$_2$(μ-H)(μ-η^2-H–SiHR). Loss of two equivalents of hydrogen from the reactive intermediates **3a,b** would generate the observed bis(μ-silylene) complexes **2a** and **2b**, respectively.

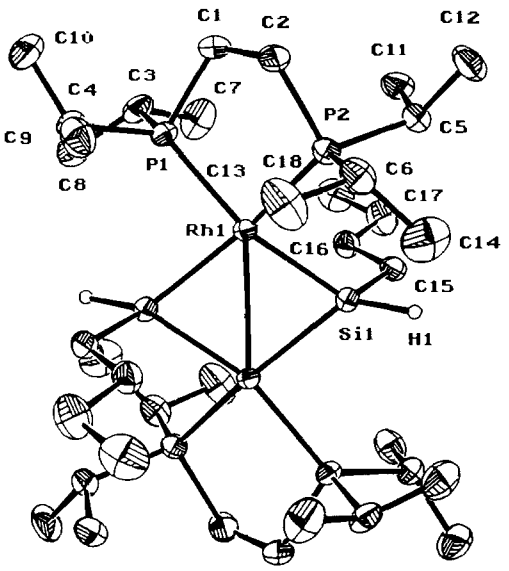

Fig. 1. Molecular structure and number scheme of *trans*-[(dippe)Rh]$_2$(μ-SiHBu^n)$_2$ (**2a**).

$$[(\text{dippe})\text{Rh}]_2(\mu\text{-H})_2 + 2\text{RSiH}_3 \xrightarrow[-\text{H}_2]{} \underset{\textbf{1}}{}$$

a: R=Bu^n
b: R=Tol^p

$$[(\text{dippe})\text{Rh(H)}]_2(\mu\text{-}\eta^2\text{-H–SiHR})_2 \quad \textbf{3a,b} \quad (2)$$

$$\downarrow -2\text{H}_2$$

$$[(\text{dippe})\text{Rh}]_2(\mu\text{–SiHR})_2 \quad \textbf{2a,b}$$

The bis(silylhydride) complexes **3a,b** can be regenerated by placing solutions of **2a,b** under an atmosphere of hydrogen. The resulting solutions are yellow, and their ^{1}H NMR spectra show resonances in the rhodium hydride region. If the excess hydrogen is removed the solutions gradually return to their original colours, and after several hours the major species in solution are again the bis(μ-silylene) complexes **2a,b**. All attempts to isolate these particular bis(silylhydride) complexes in crystalline form have failed.

$$[(\text{dippe})\text{Rh}]_2(\mu\text{-SiHR})_2 \underset{-2\text{H}_2}{\overset{+2\text{H}_2}{\rightleftharpoons}}$$

2a,b
a: R=Bu^n
b: R=Tol^p

$$[(\text{dippe})\text{Rh(H)}]_2(\mu\text{-}\eta^2\text{-H–SiHR})_2 \quad \textbf{3a,b} \quad (3)$$

The room temperature ^{31}P{^{1}H} spectrum of [(dippe)Rh(H)]$_2$(μ-η^2-H–SiHBu^n)$_2$ (**3a**) shows a single

resonance, a doublet at 84 ppm, whose broadness suggests that the molecule is fluxional in solution on the NMR time scale. The broad singlet seen in the high field, rhodium hydride region of the room temperature ^1H NMR spectrum of **3a** also supports its possible fluxionality. Variable, high temperature $^{31}P\{^1H\}$ NMR spectra confirm this fluxionality, with a sharp doublet observed at 60 °C illustrating the high temperature limit for the process. Low temperature NMR studies indicate complex behaviour of this compound in solution. These ^1H and $^{31}P\{^1H\}$ spectra are complicated and somewhat difficult to interpret; in the following discussion an attempt is made to present the most likely mechanisms for exchange and isomerism processes which are occurring.

Figure 2 shows the variable temperature $^{31}P\{^1H\}$ spectra for **3a**. The spectra show that there are actually two species in solution, and that they are both fluxional, though the coalescence point for each of the two species occurs at a different temperature. At −15 °C the broad doublet observed at room temperature has changed to two signals: a broad signal in the baseline stretching from 65 to 100 ppm and a slightly broad doublet still at 84 ppm but reduced to roughly 1/3 of the original peak height observed at room temperature. Thus the signals due to the major isomer in solution are approaching a coalescence point. This point occurs somewhere between −15 and −25 °C, where two new peaks have begun to appear on either side of the now broader doublet at 84 ppm. The integral ratios of the peaks observed at −25 °C suggest that the two isomers observed exist in a ratio of slightly more than 3:1. The peaks of the major isomer coalesce at roughly −20 °C and reach their low temperature limiting spectrum at −65 °C, where two sharp doublets at 93.6 and 75.5 ppm are observed having $^1J(Rh–P) = 150$ and 100 Hz, respectively. This pattern is similar to the one observed in the $^{31}P\{^1H\}$ NMR spectrum of $[(dippe)Rh(H)]_2(\mu\text{-}\eta^2\text{-H–SiMe}_2)_2$ at −54 °C [23]. It corresponds to there being two different types of phosphines in the complex: the signal at lower field represents the two phosphines which are *trans* to the Rh–Rh bond and the signal at higher field represents the two phosphines which are *trans* to Rh–Si bonds. A value for $\Delta G^{\ddagger}$ of 10.5 ± 0.2 kcal/mol for the process exchanging the two different types of phosphine ligands in this major isomer was calculated based on a coalescence temperature of -20 ± 5 °C. Shown below are two reasonable formulations of the major and minor isomers of **3a**,**b**; further discussion of these tentative structural proposals follows below.

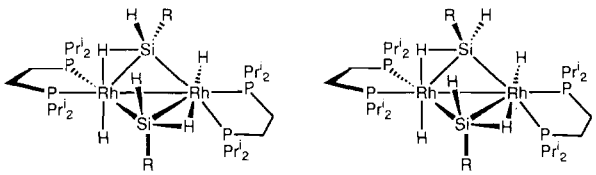

3a: R = Bu^n
3b: R = Tol^p

The $^{31}P\{^1H\}$ signal due to the minor isomer of **3a** reaches its coalescence point at approximately −55 °C. As the low temperature limit is not reached by −95 °C for these signals, and the resolution of the spectra becomes poor from −85 °C down, no activation parameters were calculated for the exchange process occurring in this isomer.

Figure 3 shows the rhodium hydride region from the variable temperature ^1H NMR spectra of **3a**. Coincidentally, these patterns look remarkably similar to those

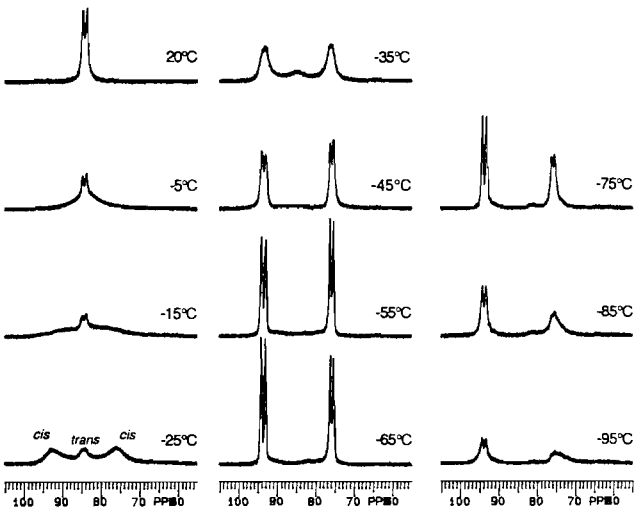

Fig. 2. Variable temperature 121.4 MHz $^{31}P\{^1H\}$ NMR spectra of $[(dippe)Rh(H)]_2(\mu\text{-}\eta^2\text{-H–SiHBu}^n)_2$ (**3a**) in C_7D_8.

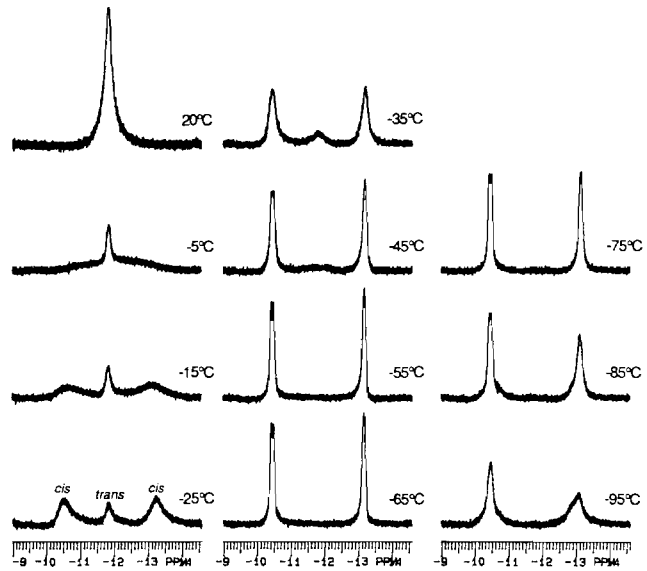

Fig. 3. Hydride region of the variable temperature 300 Mz ^1H NMR spectra of $[(dippe)Rh(H)]_2(\mu\text{-}\eta^2\text{-H–SiHBu}^n)_2$ (**3a**) in C_7D_8.

seen in the low temperature $^{31}P\{^1H\}$ NMR spectra. A broad singlet in the room temperature spectrum at −11.85 ppm collapses as the temperature is lowered to give signals due to the major and minor isomers. The signals due to the major isomer coalesce at roughly −10 °C and are most clearly resolved as two doublets due to two different types of hydride at −55 °C. It is not clear whether the agostic Si–H interactions in **3a** persist in solution or if the Si–H bonds have been oxidatively added. Both possibilities would, however, give rise to two different types of hydride ligands which are *trans* to each other at each rhodium centre. A value for $\Delta G^{\ddagger}$ (263 K) of 11.4 ± 0.2 kcal/mol was calculated for the process exchanging these two hydrides in the major isomer of **3a**. Signals due to the hydrides of the minor isomer of **3a**, which coalesce at about −45 °C, do not reach their low temperature limit in the temperature range studied. No $\Delta G^{\ddagger}$ was calculated for exchange of hydrides in this isomer.

Three stereoisomers are possible if we assume that complexes **3a,b** have the same structure as their dimethylsilane analogue; in Scheme 1, these possibilities are drawn in a simplified manner looking down the Rh–Rh vector with the phosphine ligands and the η^2-Si–H interactions removed. By analogy to allyl ligands, the substituents on silicon can be labelled *syn* or *anti*, based on the view along the Rh–Rh axis. The substituents which point to the centre, or inside, of the V-shaped core can be labelled *anti*; they are *anti* to the terminal hydrides that are *trans* to the bridging silyl groups. The substituents which point away from the core of the molecule can be labelled *syn*, as they are *syn* to the terminal hydrides. Therefore the *cis* isomer has two possible structures, wherein the substituents on the silicons are either both *syn* or both *anti*. The *trans* isomer has one R group and one hydride in an *anti* site and one of each in a *syn* site. The sterically most favoured structure, where the R groups on silicon are furthest away from each other, would probably be the *cis* isomer in which the Si–H groups are *anti* and the R groups are *syn*. The *trans* isomer should follow, with the sterically most disfavoured structure being the *cis* isomer where the R groups are *anti* and the Si–H groups are *syn*.

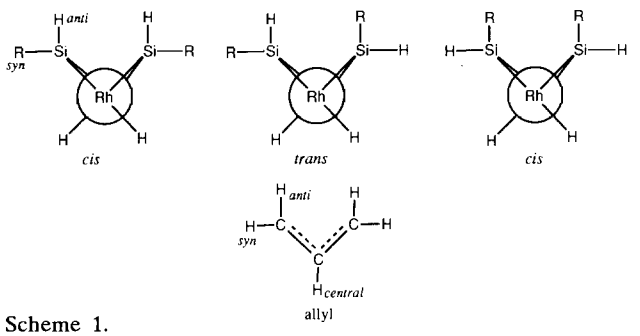

Scheme 1.

At room temperature the silyl hydride region of the ^1H NMR spectrum (Fig. 4) shows a broad singlet for the major isomer at 5.4 ppm and two broad singlets for the minor isomer at 5.1 and 4.3 ppm. These signals do not vary in their ratio as the sample is cooled; the only change is that the peaks sharpen to a minimum linewidth at -25 °C (see Fig. 4), then lose resolution gradually as the sample is further cooled. The major isomer must be a *cis* isomer (two Si–H in equivalent sites), probably with *anti* Si–H. The minor isomer is the *trans* isomer, with one *syn* Si–H (4.3 ppm) and one *anti* Si–H (5.1 ppm). We assume that the least favoured *cis* isomer is not observed.

The phosphine and hydride ligands in both isomers of **3a** could be exchanged by a mechanism involving simultaneous twisting of the two rhodium coordination spheres, as shown in Fig. 5. At each rhodium centre, the H–Rh–H axis rotates through 90°, with simultaneous breaking of one agostic Si–H bond and the formation of another. This process exchanges the terminal hydrides on rhodium and the agostic silicon hydrides. There is a concurrent twisting of the phosphine chelate rings

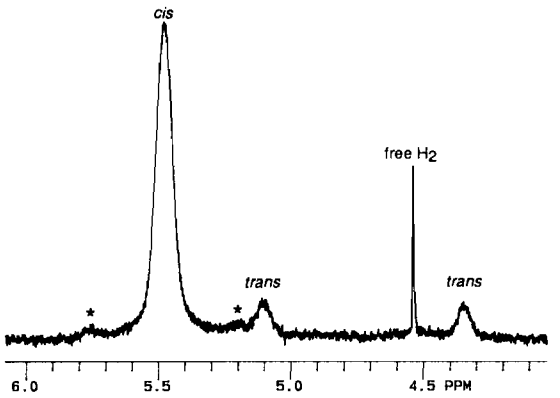

Fig. 4. Silyl hydride region of the 300 MHz ^1H NMR spectrum of **3a** at −25 °C. ^{29}Si satellites for the signal due to the *cis* isomer are indicated by an asterisk.

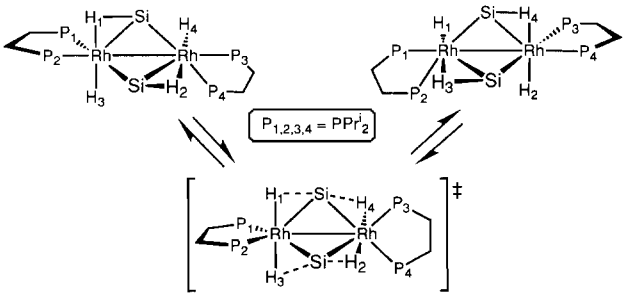

Fig. 5. Twisting mechanism which would exchange the two Rh–H sites and the two phosphine sites in compound **3** (substituents on silicon are omitted for clarity).

through 90°, which exchanges the two types of phosphorus on each ligand.

As depicted in Fig. 6(b), another mechanism that would exchange the phosphine and hydride sites in both isomers of **3a** is a 'flapping' process, whereby the 'V'-shaped core of the butterfly structure inverts, leaving the phosphines and hydrides stationary while the silicons and their substituents move. This mechanism would also exchange the *syn* and *anti* sites in the complexes, as shown in the side views of the isomers in Fig. 6(a).

Whether it is 'twisting' or 'flapping' that is actually causing exchange in $[(dippe)Rh(H)]_2(\mu\text{-}\eta^2\text{-H–SiHBu}^n)_2$ (**3a**) can be determined based on the behaviour of the Si–H resonances observed in the variable temperature ^{1}H NMR spectra. If both *cis* and *trans* isomers in solution are 'flapping', then Si–H in *syn* and *anti* sites would be exchanging and should give a single, average signal at the high temperature limit for each isomer. However, as described earlier, at room temperature this region of the ^{1}H NMR spectrum shows a broad singlet at 5.4 ppm due to the *cis* isomer and two broad singlets at 5.1 and 4.3 ppm due to the *trans* isomer. That these signals do not change at low temperature and do not vary in their ratio even when the sample is cooled to −95 °C suggests that it is the 'twisting' mechanism that best explains the data, exchanging hydrides and phosphines without exchanging the uncoordinated Si–H.

Figure 7 shows the silyl hydride region of the variable, high temperature ^{1}H NMR spectra for **3a**. The signals

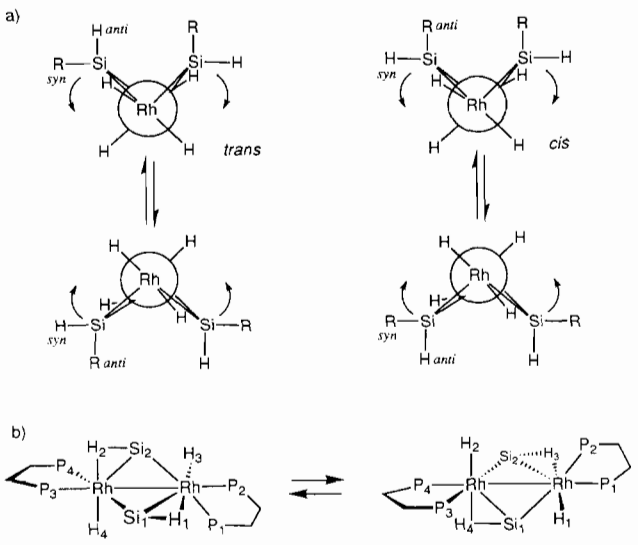

Fig. 6. (a) End views of **3a,b** demonstrating the 'flapping' mechanism which would exchange the *syn* and *anti* substituents on silicon (the phosphines are omitted for clarity). (b) A side view of the 'flapping' mechanism, showing how the two types of Rh–H and the two types of phosphines in **3** are exchanged by this mechanism (substituents on phosphorus and silicon are omitted for clarity).

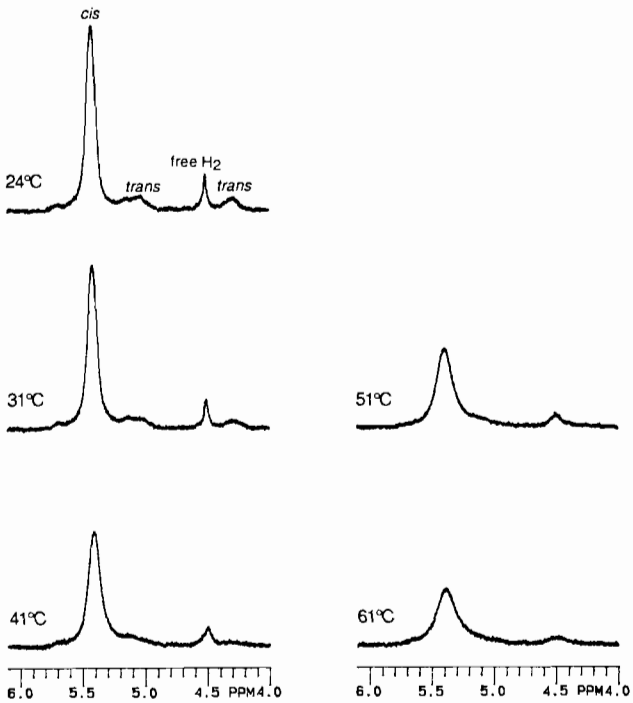

Fig. 7. Variable temperature 300 MHz ^{1}H NMR spectra of $[(dippe)Rh(H)]_2(\mu\text{-}\eta^2\text{-H–SiHBu}^n)_2$ (**3a**) in C_7D_8, showing the silyl hydride region.

for Si–H(*trans*) do broaden as the sample temperature is raised, which could be considered to be a coalescence caused by exchange of *syn* and *anti* sites in the *trans* isomer. However both the Si–H(*cis*) signal and the sharp singlet at 4.5 ppm (due to free H_2 dissolved in solution) also broaden when the sample is heated. The broad peak seen at roughly 4.5 ppm in the spectrum generated at 61 °C is not a coalescence of Si–H(*trans*) signals but is due to free H_2 in solution which is exchanging with both the *cis* and *trans* isomers of **3a**.

Generally when two different species in solution are in equilibrium the equilibrium constant, K_{eq}, is temperature dependent. Thus NMR spectra from a range of sample temperatures should show varying ratios of the two species, and integration should allow calculation of K_{eq} for each temperature. Signals for the two isomers of **3a** appear to remain in the same ratio from +60 to −95 °C, which suggests either that the two species are not in equilibrium or that K_{eq} for the isomers has a very small temperature dependence.

One experiment performed suggests that *cis*- and *trans*-**3a** should be in equilibrium. A solution containing $[(dippe)Rh]_2(\mu\text{-SiHBu}^n)_2$ (**2a**) was placed under an atmosphere of D_2. The originally red solution immediately turned yellow, indicating the formation of d_4-**3a**, $[(dippe)Rh(D)]_2(\mu\text{-}\eta^2\text{-D–SiHBu}^n)_2$. The solvent was removed under vacuum and d_6-benzene was added to the residues to make an NMR sample. Interestingly, the yellow colour of the product darkened only slightly

throughout this process: the relative slowness of this conversion of **3a** to the red $[(dippe)Rh]_2(\mu\text{-}SiHBu^n)_2$ (**2a**) is probably caused by a deuterium isotope effect on the rate of elimination of D_2 from d_4-**3a**. The important result, though, was that the ^1H NMR spectrum of this sample showed signals for both silyl hydrides and rhodium hydrides on **3a**. If there was no exchange between terminal hydrides bound to silicon and the rhodium hydrides (generated by addition of H_2 or D_2 to **2a**) then we should see only Si–H signals in this spectrum, and no rhodium hydride signals. Evidently these sites are exchanging, though the exchange must be occurring relatively slowly, as the variable temperature ^1H NMR spectra give no evidence for it. The most likely mechanism for the exchange involves dissociation of the agostic Si–H to give terminal $SiRH_2$ groups on rhodium (see Scheme 2). (This is perhaps evidence that the three-centre, two-electron Si–H interaction does exist in solution for **3a**.) Rotation around the Rh–Si bond and re-association of a different Si–H bond would exchange the terminal and 'bridging' Si–H. Note that this mechanism also changes the relative position of the R group, interchanging the *cis* and *trans* isomers. Thus there should be an equilibrium between the isomers. The temperature invariance of the equilibrium constant, K_{eq}, as observed in the variable temperature NMR studies of **3a**, may indicate that $\Delta H^\circ \approx 0$ for the conversion of one isomer to the other.

The variable temperature ^1H and $^{31}P\{^1H\}$ NMR spectra of $[(dippe)Rh(H)]_2(\mu\text{-}\eta^2\text{-}H\text{–}SiHTol^p)_2$ (**3b**) undergo the same sort of transformations as do those for **3a**, but the spectra of **3b** are much more complex. For example, from examination of the variable temperature $^{31}P\{^1H\}$ NMR spectra of **3b** (see Fig. 8), it is obvious that again there are two isomers in solution, in roughly the same ratio as they were in **3a**, presumably with the *cis* being the major isomer again. Both isomers are fluxional: the peaks due to the *cis* isomer coalesce at approximately −40 °C and are most clearly resolved at −65 °C. The peaks due to the *trans* isomer coalesce between −50 and −65 °C, and their low temperature limit is not reached by −95 °C. However, in this case the complexity of the spectra would suggest a lower symmetry in these molecules. There are more signals, and their splitting patterns indicate that $^{31}P\text{–}^{31}P$ coupling is occurring between the now inequivalent phosphines.

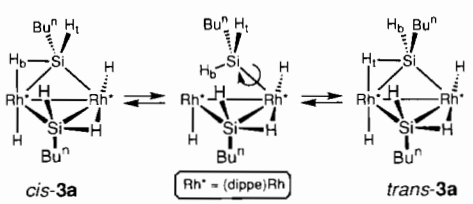

Scheme 2.

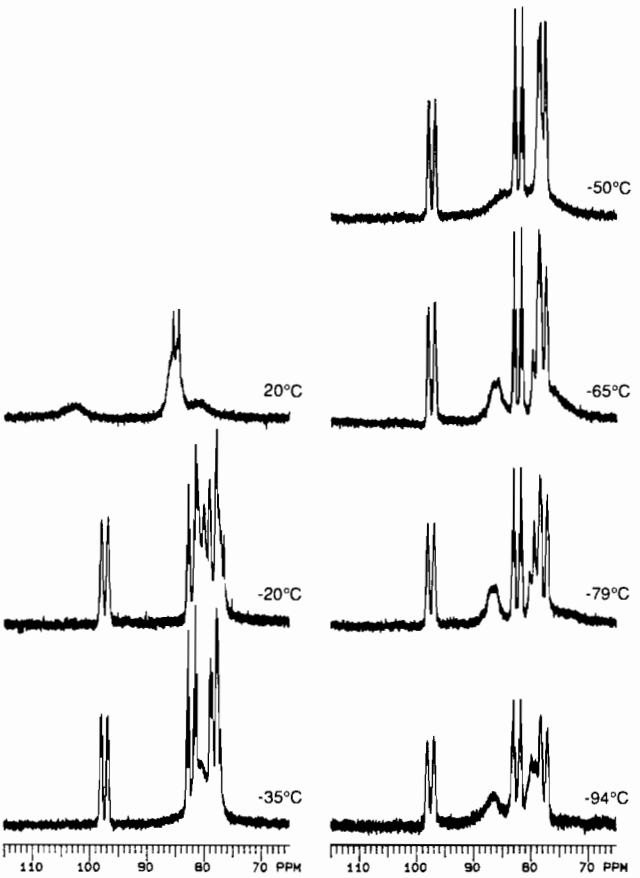

Fig. 8. Variable temperature 121.4 MHz $^{31}P\{^1H\}$ NMR spectra of $[(dippe)Rh(H)]_2(\mu\text{-}\eta^2\text{-}H\text{–}SiHTol^p)_2$ (**3b**) in C_7D_8.

These spectra are too complicated to assign; it is assumed that the decreased symmetry in **3b** arises from steric constraints imposed by the *p*-tolyl groups interacting with the isopropyl substituents on the dippe ligands. The ^1H NMR spectra of **3b** (not shown here) are correspondingly more complex in the hydride region, though Si–H signals similar to those for **3a** are seen, and the changes occurring with changes in temperature correspond to the transformations observed in the variable temperature ^1H NMR spectra of **3a**. It is therefore assumed that similar exchange processes are at work in **3b**.

Reactions of more than two equivalents of primary silanes with $[(dippe)Rh]_2(\mu\text{-}H)_2$ (1)

When 4 or 5 equiv. of a primary silane are added to $[(dippe)Rh]_2(\mu\text{-}H)_2$ (**1**) a new silicon-containing species is formed. These species, **4a,b** (where **a** = Bu^n and **b** = Tol^p), show complex ^1H and $^{31}P\{^1H\}$ NMR spectra, both at room temperature and at low temperature. Elemental analyses for the two compounds suggest the presence of three silicons per dinuclear rhodium centre for both complexes, and the resonances observed in the rhodium hydride region of the ^1H NMR spectra

and the patterns which emerge at low temperature in the $^{31}P\{^1H\}$ NMR spectra of the two compounds suggest that their structures are similar.

$$[(dippe)Rh]_2(\mu\text{-}H)_2 + \text{4–5 equiv. } RSiH_3 \xrightarrow[-3H_2]{} [(dippe)Rh]_2 \cdot (RSiH)_3(H)_2 \quad (4)$$

1 → **4a**: R=Bu^n; **4b**: R=Tol^p

The complexes **4a,b** are unusual in this system of compounds in that they can be isolated as crystalline solids which are air stable; the crystals show only slight discolouration after several days in air. These complexes are very soluble in aromatic and aliphatic solvents. In particular, **4a** is so soluble that its isolation requires the cooling of extremely concentrated pentane solutions to −40 °C. The pale yellow crystals of **4a** tend to be soft and waxy, and they easily desolvate, becoming opaque. Crystals of the *p*-tolyl analogue, **4b**, are light orange needles which are more easily isolated. An X-ray crystallographic study was carried out on a single crystal of **4b** to determine its structure; the results of this study are presented below. Figure 9 shows an ORTEP diagram of the solid-state structure of $[(dippe)Rh]_2(\mu\text{-}\eta^2\text{-H–SiHTol}^p)_2(\mu\text{-SiHTol}^p)$ (**4b**). Tables 6 and 7 show some of the relevant bond lengths and bond angles. The silicon and rhodium hydrides were located in the Fourier difference map but were not refined.

In the solid state this molecule consists of the dinuclear $[P_2Rh]_2$ unit with two rhodiums bridged by three silicon-containing ligands. One of these (Si1 in Fig. 9) is a bridging silylene unit. The other two ligands are silyl groups (Si2 and Si3) which are bound to one rhodium through a direct Si–Rh bond and to the other rhodium through participation of the Si–H bond in a three-centre, two-electron interaction with the metal centre. Examination of Rh–Si distances for each of the agostic silyl ligands in **4b** and comparison with other dinuclear complexes incorporating agostic silyl ligands suggests that oxidative addition of the Si–H bonds is arrested at an intermediate stage for Si2 and at a later stage for Si3. However, it is possible that the steric crowding at the core of **4b** as well as electronic factors could play a large role in bond length variations. The substituents on the three bridging silicons encircle the dinuclear rhodium core with alternating silicon hydride and *p*-tolyl groups. The two chelating phosphine rings are almost coplanar, there being a dihedral angle of 170.35° between the planes containing P1, P2, Rh1 and P3, P4, Rh2. The rings are tilted away from the bridging silylene ligand such that P1 and P3 are *trans* to Si1. The *trans* influence of Si1 is manifested in the P1–Rh1 and P3–Rh2 bond lengths being an average of 0.09 Å longer than the P2–Rh1 and P4–Rh2 bond lengths, respectively. The closest Si–Si interaction is 2.991 Å (Si1–Si2).

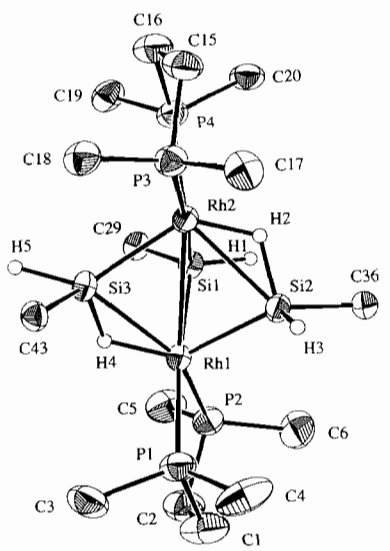

Fig. 9. Molecular structure and numbering scheme of $[(dippe)Rh]_2(\mu\text{-}\eta^2\text{-H–SiHTol}^p)_2(\mu\text{-SiHTol}^p)$ (**4b**); isopropyl groups on phosphorus and *p*-tolyl groups on silicon are represented by single carbons.

It is increasingly obvious that within this system of dinuclear rhodium silyl complexes the agostic Si–H interaction is not an exceptional phenomenon, but a standard mode of bridging ligation for silyl ligands in the solid state and probably in solution as well [14, 23]. These three-centre, two-electron interactions allow the Rh centres to increase their coordination numbers (become more coordinatively saturated) without increasing their formal oxidation state. For η^2-H_2 complexes it has been noted that very specific electronic conditions at the metal centre appear to be required for the stabilization of the η^2-H_2 form versus the dihydride formulation [26]. If the metal fragment is too basic, i.e. too electron-rich, π donation from the metal into the σ^* antibonding orbitals on H_2 will reduce the H–H bond order such that oxidative addition occurs to give two M–H bonds. However, if this backdonation is absent due to electron deficiency of the metal fragment, the coordination of the H–H σ bond is destabilized and dissociation of the hydrogen molecule occurs. The scarcity of confirmed examples of η^2-H–SiR_3 ligands seems to indicate that special electronic environments are also essential for their stabilization. Evidently the dimeric $[(dippe)Rh]_2$ fragment provides that environment, perhaps due to the basicity of the chelating phosphines with their isopropyl substituents. It is interesting to note that most of the η^2-H–SiR_3 complexes (in the system studied here, one 'R' is (dippe)Rh) that have been characterized contain strongly donating li-

gands such as trialkylphosphine ligands or coordinated arenes which are often alkyl-substituted [27, 28].

While there are some structures of dinuclear complexes reported in the literature which have two bridging silyl groups having agostic Si–H interactions [27], **4b** represents the first structurally characterized example of a dinuclear transition-metal centre having two bridging, agostic silyl ligands and a third, bridging silylene ligand as well. The ruthenium complex with three bridging dimethylsilylene ligands shown in eqn. (5) was characterized only by IR spectroscopy and mass spectrometry, by analogy with dimethylgermylene analogues of ruthenium and iron [29]. It is the only other example of a metal–metal bond bridged by three silicon-containing ligands.

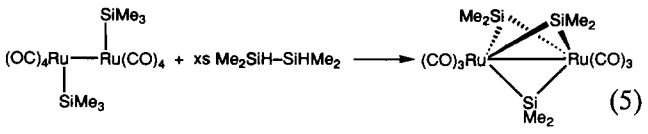

(5)

In addition, there are two crystallographically characterized complexes that contain dinuclear platinum centre with bridging ligands with a total of four silicons bound to the two metal centres; these both contain bridging disilyl ligands (eqns. (6) and (7)) [12, 30].

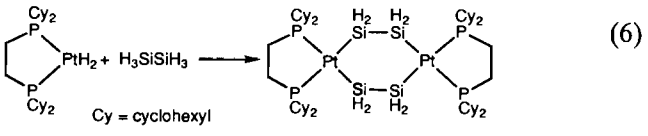

(6)

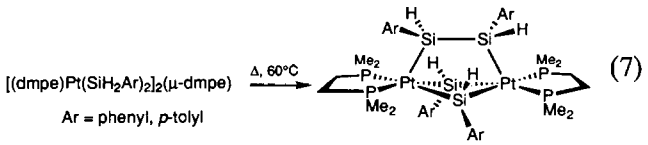

(7)

*Room and variable temperature NMR spectra of [(dippe)Rh]$_2$(μ-η^2-H–SiHR)$_2$(μ-SiHR) (R = Bu^n (**4a**), Tol^p (**4b**))*

NMR spectroscopic studies of **4a,b** have been of limited use in discerning the solution structures of these complexes. While for **4a** the spectra are generally consistent with a structure analogous to the solid-state structure of **4b**, the spectra for **4b** are somewhat more complex and difficult to assign. It is likely that **4b** does have a structure in solution which is similar to its solid-state structure, and that the complexities in its NMR spectra arise from a loss of symmetry in the complex due to the steric interactions of the *p*-tolyl groups on silicon with the isopropyl groups on the phosphine ligands.

The ^{1}H NMR spectrum of **4a** in solution is temperature invariant down to −85 °C and, as mentioned above, the structural information it provides about the complex is consistent with a structure analogous to the solid-state structure of **4b** shown in Fig. 9. Figure 10 shows the room temperature ^{1}H NMR spectrum of **4a**.

In Fig. 10, five separate resonances due to hydrides in the molecule are observed, each of relative intensity one: three of these signals occur between 6.8 and 4.5 ppm, where Si–H resonances normally occur; the other two signals appear in the high field region normally associated with Rh–H resonances. This is consistent with a structure containing three SiHBu^n fragments and two hydrides which are bound to rhodium. The shifts of the silyl hydride resonances (6.78, 6.52 and 4.59 ppm) suggest that there are two Si–H in similar chemical environments and one in a different chemical environment. ^{1}H NMR homonuclear decoupling experiments have shown that none of the five hydrides are coupled to each other. The rhodium hydride resonances are multiplets which show second order patterns. A ^{1}H{^{31}P} NMR spectrum of **4a** shows a simple doublet for each rhodium hydride signal, indicating that each hydride is coupled to just one ^{103}Rh. In the same ^{1}H{^{31}P} NMR spectrum, the Si–H resonances, seen as broad singlets in the ^{31}P-coupled spectrum, have slightly smaller $w_{1/2}$ values but no coupling is resolved. A computer simulation of the rhodium hydride signals observed in the ^{1}H NMR confirms that each hydride is coupled to a single rhodium and also to two different phosphorus nuclei. The ^2J(H–P) values range from 11 to 13 Hz, which are classic values for *cis* coupling [31].

While it is assumed that **4b** has the same structure in solution as **4a** (i.e. the same as the solid-state structure of **4b**) the room temperature spectrum of **4b** is more complex, particularly in the aromatic and Si–H regions. The changes in this spectrum as the temperature is lowered, however, are somewhat informative. A single *p*-tolyl methyl peak seen in the room temperature spectrum splits into three separate signals at low tem-

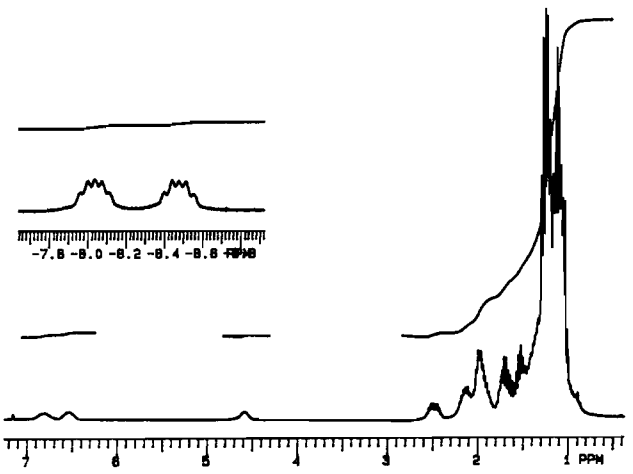

Fig. 10. Room temperature 300 MHz ^{1}H NMR spectrum of [(dippe)Rh]$_2$(μ-η^2-H–SiHBu^n)$_2$(μ-SiHBu^n) (**4a**) in C_6D_6.

perature, indicating the inequivalent environments for the three *p*-tolyl groups. The *ortho* and *meta* proton signals split accordingly in the low temperature spectrum. One of the three *p*-tolyl groups experiences restricted rotation around its Si–C_{ipso} bond, as one of the three sets of aromatic proton signals further splits from two into four separate signals when the sample is cooled. The Si–H signals become correspondingly complex with the decrease in temperature, but the rhodium hydride signal of relative intensity two (a single multiplet of the same second order pattern as is seen for the hydrides in **4a**) does not change as the temperature is lowered, apart from broadening slightly. The two rhodium hydrides must be exchanging rapidly, giving an average signal.

The $^{31}P\{^1H\}$ NMR spectrum of **4a** at room temperature shows peaks due to four inequivalent phosphines that are somewhat broad and unresolved. Figure 11 shows the variable, low temperature $^{31}P\{^1H\}$ NMR spectra of **4a**. The spectrum generated at −24 °C shows clearly the four signals. Those between 60 and 65 ppm have ^1J(Rh–P) values of 105 Hz and are due to the two phosphines *trans* to the bridging silylene ligand. Those at lower field with ^1J(Rh–P) values of about 160 Hz correspond to the phosphines which are *cis* to the bridging silylene ligand, and at this temperature the coupling between these *cis* phosphines is clearly resolved (^3J(P–P) = 53 Hz). A computer simulation of the $^{31}P\{^1H\}$ NMR spectrum of **4a** at −24 °C confirms these assignments (see 'Experimental'). As the sample is further cooled to a minimum of −83 °C more splitting of the four peaks is observed. This splitting may be due to an equilibrium which is established at low temperature between two different conformers in solution. No corresponding splitting is observed in the variable temperature ^1H NMR spectra, so either the changes in conformation do not significantly alter the proton environments in **4a**, or the shift differences for the ^1H NMR signals due to the two conformers are too small for separate peaks to be resolved at low temperature.

While the broadness of the peaks in the room temperature $^{31}P\{^1H\}$ NMR spectrum of **4a** might suggest that the four magnetically inequivalent phosphorus nuclei are exchanging, in fact the peaks are simply broad and do not show a chemical shift dependence on temperature. At higher temperatures, $^{31}P\{^1H\}$ NMR spectra (not shown here) show the four signals getting slightly broader, then sharpening as the sample is heated to 70 °C. Evidently the broadening of the $^{31}P\{^1H\}$ NMR signals is due to some other process (perhaps having to do with movement of the n-butyl groups on silicon) than exchange of the phosphine ligands.

The variable, low temperature $^{31}P\{^1H\}$ spectra of [(dippe)Rh]$_2$(μ-η^2-H–SiHTol^p)$_2$(μ-SiHTol^p) (**4b**) are shown in Fig. 12. The room temperature spectrum shows two very broad peaks superimposed on each other, centred at 70 ppm. Each peak represents two phosphines which are exchanging with each other. Lowering the temperature to −30 and to −45 °C causes these two signals to separate into four distinct signals in a pattern almost identical to that of the spectrum of **4a** at −24 °C, indicating that the two molecules

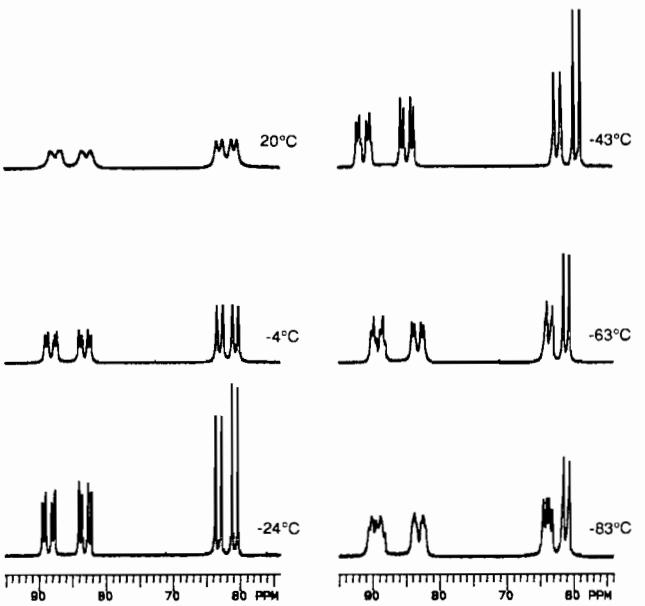

Fig. 11. Variable temperature 121.4 MHz $^{31}P\{^1H\}$ NMR spectra of [(dippe)Rh]$_2$(μ-η^2-H–SiHBu^n)$_2$(μ-SiHBu^n) (**4a**) in C_7D_8.

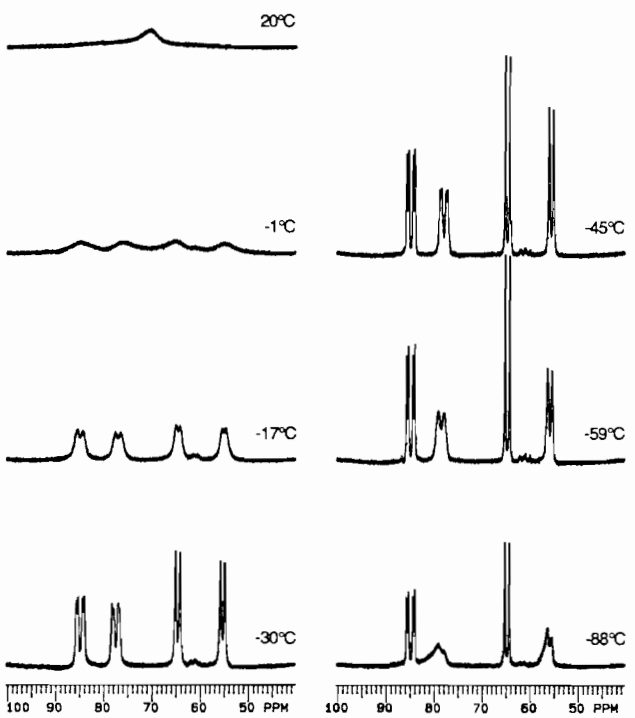

Fig. 12. Variable temperature 121.4 MHz $^{31}P\{^1H\}$ NMR spectra of [(dippe)Rh]$_2$(μ-η^2-H–SiHTol^p)$_2$(μ-SiHTol^p) (**4b**) in C_7D_8.

have fairly similar structures in solution, with four inequivalent phosphines. As the temperature of **4b** is lowered further to −88 °C, though, the peaks behave differently from those due to **4a**. The two low field signals initially show splitting which indicates that those two phosphines are coupled to each other; these are the phosphines which are *cis* to the bridging silylene ligand. However, as the sample temperature is lowered the upfield signal of this pair and the upfield signal of the other pair of signals begin to broaden and become slightly skewed. It looks as though signals due to a new species are growing in, but in this case the downfield signals of each pair remain perfectly sharp, with no loss of coupling. It is almost as though only one chelating phosphine ligand is undergoing some conformational exchange while the other remains fixed, though it is difficult to imagine how any conformational change on one side of the molecule could leave the other side unaffected.

It is possible that the exchange of phosphorus nuclei indicated by the variable temperature $^{31}P\{^1H\}$ NMR spectra of **4b** are caused simply by the fluxionality of the rhodium hydrides in this complex. If **4b** does have the same structure in solution as it does in the solid state, then there are two types of phosphorus donors in the complex: one type (P2, P4) is *cis* to the bridging silylene ligand (Si1), the other type (P1, P3) is *trans* to the silylene ligand. Within each category the only difference between the two phosphorus nuclei is their spatial relationship with the substituents on the two bridging silyl ligands.

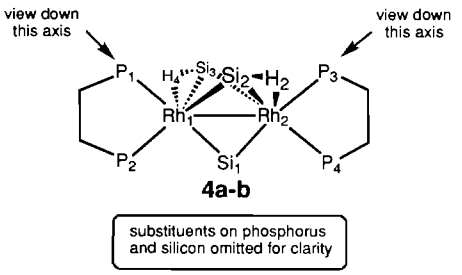

Shown in Scheme 3 are end views of the complex, looking along the two P_{trans}–Rh–$Si_{silylene}$ axes. These views demonstrate that both P1 and P3 are *cis* to an agostic Si–H bond, but the arrangement of the Si–R and uncoordinated Si–H groups on the agostically-bound silicon is different for these two views. If the hydrides (presumably agostic in solution, or, if terminal, *cis* to a particular bridging silicon) shift from being associated with one silyl ligand to the other, this would exchange P1 and P3 and between these two inequivalent magnetic environments, as shown in Scheme 3. Thus P1 and P3 are exchanged by this simple hydride shift, as are P2 and P4. The only problem with this proposed mechanism of fluxionality for **4b** in solution is the lack of supporting evidence in the ^1H NMR spectra.

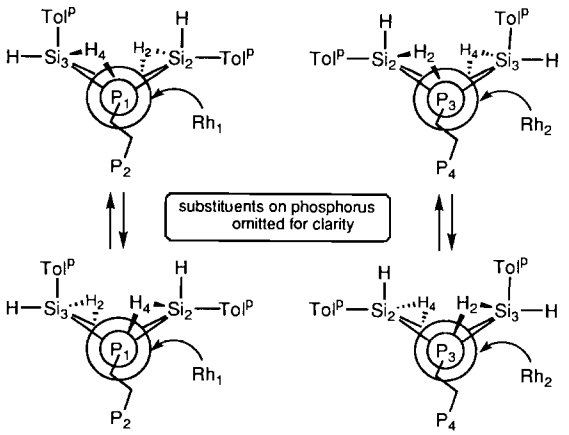

Scheme 3.

Hydride exchange around the entire core may be responsible for the different types of structure observed by $^{31}P\{^1H\}$ NMR spectroscopy for complexes **4a,b** in solution at low temperature, though the fact that the rhodium hydride signals in the ^1H NMR spectra do not change for either of **4a,b** at low temperature is not consistent with this exchange. Another possibility is simply that, at low temperature in solution, the interaction of the isopropyl groups on the chelating phosphines with the substituents on silicon in these complexes causes them to 'lock' into two subtly different conformations where the phosphines are twisted slightly and uniquely relative to the ligands bridging the two rhodiums.

The stoichiometric chemistry of primary silanes with the dinuclear hydride **1** is clearly very complex. The fact that these complexes form via Si–H bond activation with expulsion of H_2, the latter process occurring via H–H bond formation, is yet another example of the close connection between silanes and dihydrogen. A further complicating feature of this system is the fluxional processes that these highly silylated dinuclear rhodium complexes display. The fact that there are six magnetically active spins in the $^{31}P\{^1H\}$ NMR spectra (four ^{31}P and two ^{103}Rh) does provide some information on likely exchange mechanisms; however, more often than not these nuclei couple to generate complex second-order spectra that can be ambiguous. What does emerge from these studies is that activation of Si–H bonds and H–H bonds is facile within the dinuclear framework. As will be seen in the next section, Si–Si bond formation is also facile for these systems.

Dehydrogenative silicon–silicon coupling of primary silanes in the presence of catalytic amounts of [(dippe)Rh]$_2$(μ-H)$_2$ (1)

The activity of primary silanes toward Si–Si coupling using [(dippe)Rh]$_2$(μ-H)$_2$ (**1**) as catalyst was investigated using *p*-tolylsilane and n-butylsilane as substrates. The

two silanes behaved very differently under the catalytic conditions, and the results of these studies suggest that more attention should be paid to the use of late transition-metal catalysts for the coupling reactions of primary alkylsilanes as opposed to the arylsilanes normally used.

When a catalytic amount of $[(dippe)Rh]_2(\mu\text{-}H)_2$ (**1**) is added to a solution of *p*-tolylsilane in toluene, the dark green colour of the catalyst precursor immediately changes to a golden colour, and bubbles are evolved (H_2) (eqn. (8)). The formation of bubbles slows after several hours. Analysis of the reaction mixture by GC-MS shows very similar results to those observed for the catalytic reaction of phenylsilane with Wilkinson's catalyst; that is, very low conversion of the monomer to the disilane and various products from simultaneous disproportionation reactions. In general, these product distributions are not particularly reproducible. Obvi-

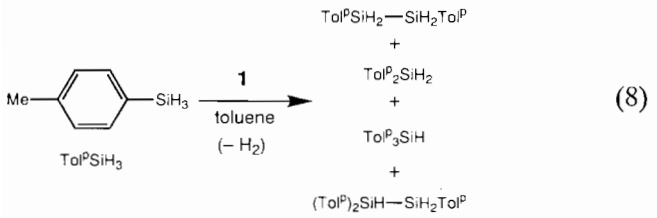

(8)

ously SiH_4 must be forming as well, as a disproportionation product, but is evolved along with the hydrogen formed during the coupling reactions.

The reaction of n-butylsilane with catalytic amounts of **1** does not, under mild conditions, give any disproportionation products. Instead, dehydrogenative coupling proceeds cleanly, giving much higher conversions of monomer (63%), and giving polysilane products with chains up to five silicons long (eqn. (9)).

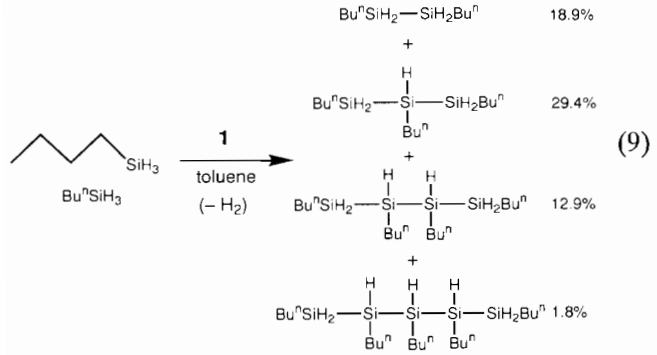

(9)

Though the yield of the higher chains is low, these are the longest chains obtained from coupling of a monosilane using a platinum-group catalyst [32, 33]*.

*Ref. 33 claims the use of chloroplatinic acid as a catalyst for the dehydrogenative coupling of hexylsilane to oligomeric silanes up to five silicons long; however, the reaction conditions include the use of oxygen which may result in the formation of siloxanes rather than silane type products. For confirmation of this see ref. 32.

Mechanistic considerations in the dehydrogenative coupling of primary silanes

As already mentioned in 'Introduction', the mechanism for the dehydrogenative coupling of silanes catalyzed by late transition-metal complexes is not known, but is presumed to proceed via oxidative addition and reductive elimination steps [1]. Figure 13 shows a possible catalytic cycle involving late transition-metal hydride complexes [10]. Obviously the metal hydride species (top of the catalytic cycle) must be coordinatively unsaturated for the reaction to proceed. All of the steps in this cycle have at one time or another been observed to occur stoichiometrically, though not all have been observed for one particular metal system [2]. Given that at some point in the catalytic cycle both of the silanes that are coupling to each other must be bound to the metal centre it is easy to see that the steric requirements of the silane will have a large effect on the progress of the reaction. This explains why secondary silanes usually give only dimers in these reactions, as the formation of longer chains demands the coordination of both a secondary silane and a tertiary disilane to the metal centre. Similarly, it seems more likely that a primary silane would undergo coupling reactions with its dimers and trimers to give longer chains; this only requires simultaneous activation of a primary silane and a secondary polysilane. Thus formation of longer polysilane chains should be possible using late transition-metal catalysts, as long as the monomer chosen is not inclined to participate in the competing disproportionation reactions, as are many arylsilanes.

It is interesting to speculate on the possible involvement of a dinuclear rhodium species in the catalytic silicon–silicon coupling cycle for the system studied here. The stoichiometric chemistry of silanes with $[(dippe)Rh]_2(\mu\text{-}H)_2$ (**1**) contains examples of almost all the steps in the catalytic cycle shown in Fig. 13, yet they occur at the dinuclear centre and generate dinuclear products in all cases: oxidative addition of a silane to a metal hydride, hydrogen elimination and addition of

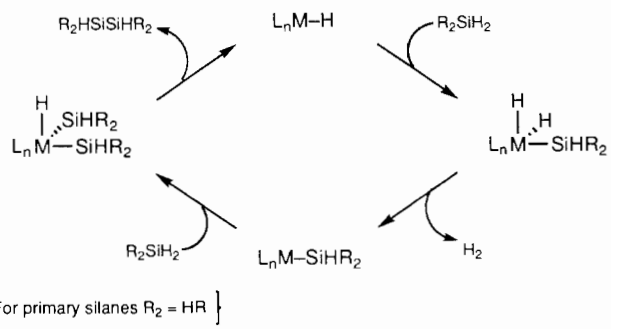

Fig. 13. Mechanism for the dehydrogenative coupling of silanes catalyzed by late transition-metal complexes, based on oxidative addition and reductive elimination steps.

a silane to a metal silyl complex. The last reaction occurs twice for primary silanes, as the complexes **4** almost certainly form from the addition of silane to a bis(μ-silylene) complex, **2**, or a bis(silylhydride) complex, **3**. The only step which has not been clearly observed to occur stoichiometrically in this system (apart from the addition of a single equivalent of primary silane to **1**) is the reductive elimination of an Si–Si bond, though the reverse reaction has been observed in the addition of 1,1′,2,2′-tetraphenyldisilane to **1**, where cleavage of the Si–Si bond gives [(dippe)Rh]$_2$(μ-H)(μ-η^2-H–SiPh$_2$) [23]. Certainly there has been no direct evidence of any mononuclear species forming in any of the reactions of **1** with silanes. This does not preclude the possible fragmentation of dinuclear compounds into highly active mononuclear species which recombine after participation in the catalytic cycle, but the fact that dinuclear complexes are capable of almost all the steps required for a catalytic cycle does support the idea of a dinuclear catalyst. The low yields of the longer chains and the fact that odd-numbered chain lengths occur suggest that the chain growth is stepwise. For chains longer than two silicons, this requires addition of both a monomer and an oligomer Si–H bond to the active catalyst. This could be facilitated by having two Rh centres in the catalyst at which the additions could occur. It is possible that a dinuclear bis(silylhydride) complex could be involved in the further coupling of a primary silane, for example where one bridging group is an η^1-disilane as in compound **A**.

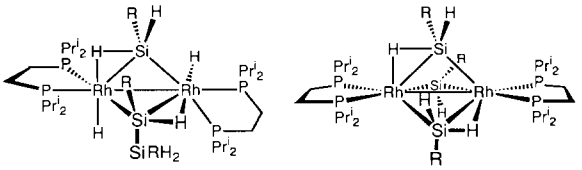

A **4**

Elimination of an Si–Si bond from this intermediate would generate the trimer plus **1**, which would react rapidly with more silane. Figure 14 shows a possible mechanism for the dehydrogenative coupling of a primary silane catalyzed by **1**. Though [(dippe)Rh]$_2$(μ-η^2-H–SiHR)$_2$(μ-SiHR) (**4**) is shown as being outside the catalytic cycle in Fig. 14 this compound cannot be ruled out as a possible intermediate in the catalytic cycle. The silicons are in close proximity in this molecule, and elimination of disilane from this crowded complex could possibly drive the catalytic cycle.

In support of the notion of dinuclear centres being involved in catalytic coupling of silanes it should be noted that many reactions of silanes with mononuclear metal fragments give dinuclear metal complexes as products [4, 12, 30, 34–37]. Of note are a series of dinuclear platinum complexes in which the bridging

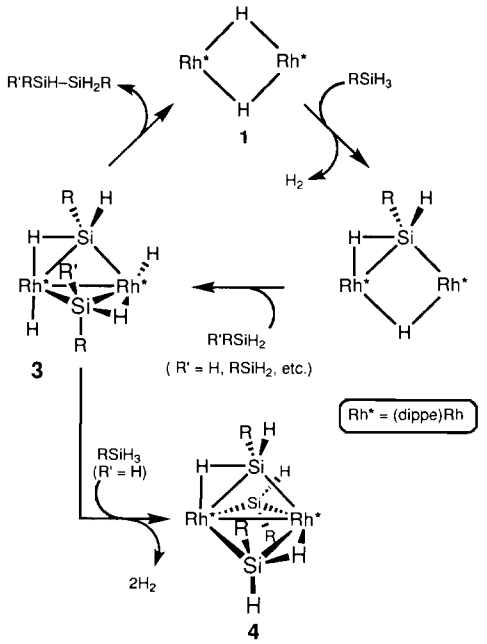

Fig. 14. Mechanism for the dehydrogenative coupling of primary silanes catalyzed by [(dippe)Rh]$_2$(μ-H)$_2$ (**1**) based on oxidative addition and reductive elimination steps at the dinuclear centre.

silylene groups are close enough to each other across the four-membered metallocycle that nascent Si–Si bond formation has been invoked [37]. Also of interest is the dinuclear platinum complex shown in eqns. (7) and (10) [12].

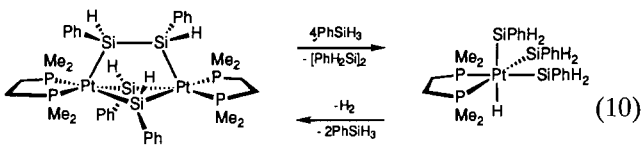

(10)

Stoichiometric Si–Si bond formation is only seen when this dinuclear 'basket' compound is formed, or upon production of the corresponding dinuclear bis(μ-silylene) complexes. The forward and backward reactions shown in eqn. (10) could be a catalytic cycle, as both of the complexes shown do act as catalyst precursors for the slow dimerization of phenylsilane.

It is important to re-emphasize that while some stoichiometric chemistry may implicate dinuclear complexes as the active species in the dehydrogenative Si–Si coupling reactions observed for this dinuclear rhodium system, these complexes may actually be side products in the catalytic cycle which must fragment in order to participate in the cycle. In the absence of kinetic data to support the activity of the dinuclear species towards the dehydrogenative coupling it is impossible to prove the involvement of dinuclear complexes in the catalytic cycle.

Supplementary material

Calculated and observed structure factor amplitudes together with a complete list of atomic coordinates and thermal parameters for **2a** and **4b** are available from the authors.

Acknowledgements

We thank Johnson Matthey for the generous loan of $RhCl_3$. Financial support for this research was provided by NSERC of Canada.

References

1 T.D. Tilley, *Acc. Chem. Res., 26* (1993) 22.
2 T.D. Tilley, *Comments Inorg. Chem., 10* (1990) 37.
3 J.Y. Corey, in G.L. Larson (ed.), *Advances in Silicon Chemistry,* Vol. 1, JAI, Greenwich, Connecticut, 1991, pp. 327–387.
4 C.T. Aitken, J.F. Harrod and E. Samuel, *J. Am. Chem. Soc., 108* (1986) 4059.
5 H.G. Woo, R.H. Heyn and T.D. Tilley, *J. Am. Chem. Soc., 114* (1992) 5698.
6 I. Ojima, S. Inaba and T. Kogure, *J. Organomet. Chem., 55* (1973) C7.
7 K.A. Brown-Wensley, *Organometallics, 6* (1987) 1590.
8 J.Y. Corey, L.S. Chang and E.R. Corey, *Organometallics, 6* (1987) 1595.
9 M. Tanaka, T. Kobayashi, T. Hayashi and T. Sakakura, *Appl. Organomet. Chem., 2* (1988) 91.
10 M.D. Curtis and P.S. Epstein, *Adv. Organomet. Chem., 19* (1981) 213.
11 E.A. Zarate, C.A. Tessier-Youngs and W.J. Youngs, *J. Am. Chem. Soc., 110* (1988) 4068.
12 R.H. Heyn and T.D. Tilley, *J. Am. Chem. Soc., 114* (1992) 1917.
13 W. Wang and R. Eisenberg, *J. Am. Chem. Soc., 112* (1990) 1833.
14 M.D. Fryzuk, L. Rosenberg and S.J. Rettig, *Organometallics, 10* (1991) 2537.
15 M.D. Fryzuk, D.H. McConville and S.J. Rettig, *J. Organomet. Chem., 445* (1993) 245.
16 M.D. Fryzuk, T. Jones and F.W.B. Einstein, *Organometallics, 3* (1984) 185.
17 M.P. Doyle, D.J. DeBruyn, S.J. Donnelly, D.A. Kooistra, A.A. Odubela, C.T. West and S.M. Zonnebelt, *J. Org. Chem., 39* (1974) 2740.
18 R.A. Benkeser, H. Landesman and D.J. Foster, *J. Am. Chem. Soc., 74* (1952) 648.
19 W.H. Campbell, T.K. Hilty and L. Yurga, *Organometallics, 8* (1989) 2615.
20 W.A. Thomas, *Annu. Rev. NMR Spectrosc., 1* (1968) 43.
21 *teXsan: Crystal Structure Analysis Package,* Molecular Structure Corporation, The Woodlands, TX, 1985 and 1992.
22 *International Tables for Crystallography,* Vol. C, Kluwer, Boston, MA, 1992, pp. 200–206 and 219–222.
23 M.D. Fryzuk, L. Rosenberg and S.J. Rettig, unpublished results.
24 B.K. Nicholson, K.M. Mackay and R.F. Gerlach, *Rev. Silicon, Germanium, Tin, Lead Compd., 5* (1981) 67.
25 G. Hencken and E. Weiss, *Chem. Ber., 106* (1973) 1747.
26 P.G. Jessop and R.H. Morris, *Coord. Chem. Rev., 121* (1992) 155.
27 U. Schubert, *Adv. Organomet. Chem., 30* (1990) 151.
28 H. Suzuki, T. Takao, M. Tanaka and Y. Moro-oka, *J. Chem. Soc., Chem. Commun.,* (1992) 476.
29 A. Brookes, S.A.R. Knox and F.G.A. Stone, *J. Chem. Soc. A,* (1971) 3469.
30 M.J. Michalczyck, C.A. Recatto, J.C. Calabrese and M.J. Fink, *J. Am. Chem. Soc., 114* (1992) 7955.
31 W.E. Piers, *Ph.D. Thesis,* University of British Columbia, 1988.
32 C.A. Tessier *et al.,* in J.F. Harrod and R. Laine (eds.), *Inorganic and Organometallic Oligomers and Polymers,* Kluwer, Dordrecht, Netherlands, 1991, pp. 13–22.
33 A. Onopchenko and E.T. Sabourin, *J. Org. Chem., 52* (1987) 4118.
34 M. Auburn, M. Ciriano, J.A.K. Howard, M. Murray, N.J. Pugh, J.L. Spencer, F.G.A. Stone and P. Woodward, *J. Chem. Soc., Dalton Trans.,* (1980) 659.
35 M.J. Bennett and K.A. Simpson, *J. Am. Chem. Soc., 93* (1971) 7156.
36 M.M. Crozat and S.F. Watkins, *J. Chem. Soc., Dalton Trans.,* (1972) 2512.
37 E.A. Zarate, C.A. Tessier-Youngs and W.J. Youngs, *J. Chem. Soc., Chem. Commun.,* (1989) 577.